JOURNAL OF GUIDANCE, CONTROL, AND DYNAMICS
Vol. 35, No. 1, January–February 2012

Instantaneous Ambiguity Resolution in Global-Navigation-Satellite-System-Based Attitude Determination Applications: A Multivariate Constrained Approach

Gabriele Giorgi*
Delft University of Technology, 2629 HS Delft, The Netherlands
Peter J. G. Teunissen†
Curtin University of Technology, Perth, Western Australia 6102, Australia
and
Sandra Verhagen‡ and Peter J. Buist§
Delft University of Technology, 2629 HS Delft, The Netherlands

DOI: 10.2514/1.54069

Carrier phase integer ambiguity resolution is the key to high-precision Global Navigation Satellite System (GNSS) positioning, navigation, and attitude determination. It is the process of resolving the unknown cycle ambiguities of the carrier phase data as integers. After ambiguity resolution, precise baseline estimates become available, which can be used to derive the attitude of a multi-antenna platform. The purpose of this contribution is to present and test a rigorous GNSS-based attitude determination method, optimally exploiting the complete set of geometrical constraints. The key to this new method is an extension of the popular LAMBDA method: the multivariate constrained LAMBDA. The method estimates the integer ambiguities and the platform's attitude in an integral manner, fully exploiting the known body geometry of the multi-antenna configuration. As a result, the ambiguity resolution performance is greatly improved. The method is extensively tested addressing the most challenging scenario: single-epoch single-frequency GNSS observations are processed without any filtering, external aid, or dynamic modeling.

I. Introduction

GLOBAL-NAVIGATION-SATELLITE-SYSTEM (GNSS)-based attitude determination employs multiple antennas firmly mounted on a body in order to estimate its orientation with respect to a given reference frame. Many studies have already been carried out to investigate the feasibility and performance of multiantenna GNSS receivers as attitude sensors [1–16]. Attitude estimation via GNSS observations is demonstrated to be a viable technique with a wide spectrum of challenging applications, ranging from terrestrial to maritime (guidance of land vehicles, precise docking of vessels, and precision farming), and from air to space (landing assistance, unmanned air vehicles, and space platforms guidance and control) [1–3,11,12,17–22].

High-precision GNSS-attitude determination requires the use of the carrier phase observations, which provide higher range measurement accuracy than the code observables but are ambiguous by an unknown integer number of cycles. Integer ambiguity resolution is the process of resolving these unknown ambiguities as integers.

Integer ambiguity resolution is a nontrivial problem, especially if one aims at developing reliable and fast techniques ultimately capable of instantaneous correct fixing. Various ambiguity resolution methods have been developed, differing in the way the problem is approached and solved. The earliest strategies for attitude ambiguity resolution were the so-called motion-based methods [4,23–25]. These methods take advantage of the change in receiver-satellite geometry partially induced by the platform motion. However, these methods are not applicable on an epoch-by-epoch basis, since motion of the platform is a prerequisite. Another class of methods are the search-based methods. These methods do not depend on motion and can be applied instantaneously (for further discussion, see [9,26] and references therein). Several search-based methods make use of the integer least-squares (ILS) estimators [27], which extend the least-squares theory to linear models where a subset of the unknowns is integer valued. A widely used ILS implementation is the least-squares ambiguity decorrelation adjustment (LAMBDA) method [28], which is currently the standard method for solving unconstrained GNSS ambiguity resolution problems [29–33]. For unconstrained and linearly constrained GNSS models, the method is known to be optimal in the sense that it provides the highest possible success rate in a numerically efficient way [34–36]. Although the standard LAMBDA method has been used for attitude determination [6,10,14,37–39], it is not designed for rigorously solving such nonlinearly constrained problems. Incorporating the known body frame geometry of the GNSS antennas into the integer estimation process results in a nonlinear mixed estimation problem. The nonlinear constraints originate from the a priori knowledge of the length and orientation of the baselines. It is the purpose of this work to provide and test the rigorous solution of the nonlinearly constrained ILS problem.

First, the inclusion of a baseline-length constraint for two-antenna configurations was analyzed and tested: observations from two antennas separated by a known distance were processed including the baseline-length constraint, resulting in a large increase in success rate [40,41]. In case several antennas are installed aboard a platform, one may benefit from the additional a priori constraints on the mutual baseline orientations in the body frame. Instead of separately accounting for all the different constraints, the problem can be

Presented at the IEEE/AIAA Aerospace Conference, Big Sky, MT, 6–13 March 2010; received 22 February 2011; revision received 21 April 2011; accepted for publication 21 April 2011.

*Researcher, Delft Institute of Earth Observation and Space Systems, Kluyverweg 1; G.Giorgi@TUDelft.nl.

†Professor, ARC Federation Fellow, Head of GNSS Research Laboratory, Department of Spatial Sciences, Kent Street, Bentley; P.Teunissen@Curtin.edu.au.

‡Professor, Delft Institute of Earth Observation and Space Systems, Kluyverweg 1; A.A.Verhagen@TUDelft.nl.

§Researcher, Delft Institute of Earth Observation and Space Systems, Kluyverweg 1; P.J.Buist@TUDelft.nl.

reformulated by recognizing that the baseline coordinates in the body frame are related to the coordinates in any given orthonormal[¶] frame via a rotation matrix. The constraints are implicitly embedded in the orthonormality of the rotation matrix, which preserves the distances between points after the transformation. An underlying assumption is that the antennas are mounted on a rigid platform.

The ILS theory applied to a linear model where a subset of the unknowns is integer valued and another subset has to respect a nonlinear geometrical constraint was recently analyzed [42]. The proposed implementation, based on the efficient LAMBDA method, was coined the multivariate constrained LAMBDA (MC-LAMBDA) method. Existing approaches either first resolve the ambiguities and then use the precise baseline estimates for attitude determination [5,10,43], or they use the baseline-length constraints only for validation purposes [8,38,44]. The essential difference with both classical approaches is that the new algorithm solves for the integer ambiguities and body attitude in an integral manner, tremendously aiding the search for the correct integer ambiguities.

In this contribution, the principles of the MC-LAMBDA method are reviewed, and its performance is tested by means of simulations and static, low-dynamic, and high-dynamic experiments. The most challenging application is addressed: single-epoch single-frequency (SE–SF) GPS-only full attitude ambiguity resolution. Single-epoch performance is extremely important for dynamic platforms, where a quick recovery from changes of tracked satellites, cycle slips, and losses of lock is necessary to avoid undesired loss of guidance. The single-frequency case is of interest for many aerospace applications, where limits on weight and power consumption must often be respected.

The structure of this contribution is as follows. Section II deals with the underlying theory. First, the GNSS-based attitude model is introduced, including a review of commonly used parameterizations of the attitude matrix. Next, the rigorous least-squares solution of the GNSS-attitude model is presented and the problem of estimating the orthonormal attitude matrix is analyzed. The performance of the MC-LAMBDA method is assessed based on tests with various data sets. First, simulated data with a priori noise levels and number of observations are processed (Sec. III). This allows us to precisely test the method performance in terms of success rate and, all conditions being equal, to make a sound comparison between the LAMBDA and the MC-LAMBDA methods. Results obtained from two static experiments are described in Sec. IV: these experiments differ by test location, receiver grades, and baseline lengths employed. Finally, Sec. V presents the test results for dynamic platforms, namely, a sailing boat and a flying aircraft.

II. Constrained Integer Least Squares for GNSS-Attitude Determination

This section deals with the functional and stochastic GNSS observation models. The code and carrier phase measurements are cast in a linear(ized) model for which the unknowns are the integer ambiguities and the entries of the orthonormal attitude matrix. The resulting mixed model is efficiently solved with an extension of the LAMBDA method, named the MC-LAMBDA method.

A. Multivariate GNSS-Attitude Model

1. Multivariate Functional Model for GNSS Observations

The single-frequency GNSS code and carrier phase measurements are obtained from tracking $n+1$ satellites. These observations are affected by errors, originating both at the satellite and at the receiver sides, such as clock biases, instrumental delays, and multipath. Moreover, the signals propagate through the atmosphere, which affects the propagation differently in the ionospheric and in the tropospheric layers. These errors are mitigated in relative positioning models, where simultaneous measurements from two or more antennas are available. It is then possible to construct so-called double difference (DD) carrier phase and code observations by taking the differences between observations collected at two antennas from two different satellites. In this way, the clock errors, biases, and instrumental delays become negligible, and the number of unknowns to be determined is reduced [45]. Furthermore, the atmospheric errors are eliminated in case of short baselines, since the signals travel approximately the same path from the satellites to the closely separated antennas.

Assuming a set of $2n$ DD observations, the functional and stochastic models are [45–49]

$$y = Az + Gb + \epsilon; \qquad D(y) = Q_{yy} \qquad z \in \mathbb{Z}^n; \qquad b \in \mathbb{R}^c \quad (1)$$

where y is the vector of DD carrier phase and code observables (order $2n$), z is the integer vector of n ambiguities (expressed in cycles), b is the vector of remaining c real-valued unknowns, and ϵ contains the unmodeled errors, mostly consisting of random noise and multipath. No attempt is made to model or attenuate the effect of the latter in the estimation process. It is assumed that the separation between the antennas is limited to a few 100 meters, so that the atmospheric parameters can be neglected. Hence, the three baseline coordinates are the only real-valued unknowns ($c = 3$). A is the $(2n \times n)$ design matrix that contains the carrier wavelength λ, $A = [1, 0]^T \otimes \lambda I_n$, whereas G is the $(2n \times 3)$ matrix of differenced unit line-of-sight vectors, $G = [1, 1]^T \otimes [u_1, \ldots, u_n]^T$, with $\otimes$ as the Kronecker product. A Gaussian error on the observables is assumed: the dispersion on the vector of observables $D(y)$ is described by the $(2n \times 2n)$ variance–covariance (V–C) matrix Q_{yy}.

For full attitude determination, at least three antennas are required. Therefore, model (1) is extended to cast the observations collected with a multiantenna system and to directly link the observations to the unknown attitude matrix. For this purpose, consider a set of $m+1$ antennas tracking the same $n+1$ GNSS satellites. The GNSS DD observations formed with the m independent baselines are cast into the multivariate model [42]

$$Y = AZ + GB + \Xi; \qquad D(\mathrm{vec}(Y)) = Q_{YY}$$
$$Z \in \mathbb{Z}^{n \times m}; \qquad B \in \mathbb{R}^{3 \times m} \quad (2)$$

where Y is the $(2n \times m)$ matrix for which the columns contain the DD code and phase observations from each baseline. The m columns of Z are the vectors (order n) of integer-valued ambiguities, and B is the $(3 \times m)$ matrix of real-valued baseline coordinates. Ξ is the $(2n \times m)$ matrix of unmodeled errors. Because of the short baselines hypothesis, the deviations between the different line-of-sight vectors from each antenna are disregarded; hence, the same matrix of line-of-sight vectors G is used.

To define the V–C matrix of the matrix of observables Y, the vec operator is applied: it stacks the columns of the $2n$ by m matrix Y into the vector $\mathrm{vec}(Y)$ of order $2nm$, for which the dispersion is then described by the $(2nm \times 2nm)$ V–C matrix Q_{YY}.

2. GNSS-Attitude Model

The antennas are assumed to be firmly mounted on the same rigid platform, and their local coordinates are known beforehand; that is, the baseline lengths and relative orientations of the baselines are known and constant. The hypothesis of constant length constrains the extremity of each baseline vector to lie on the surface of a sphere having a radius equal to the baseline length, thus reducing the number of independent baseline coordinates from $3m$ to $2m$. Additionally, the baseline relative orientations are known, so that the set of admissible baseline coordinates can be described by means of a rigid rotation and, consequently, the number of degrees of freedom for the baseline coordinates is further reduced from $2m$ to three (two in the special case of a single baseline).

The body frame $e_1 e_2 e_3$ is defined to describe the antenna coordinates on the platform in a local coordinate system. The matrix of local baseline coordinates F is built as follows: the first axis e_1 is aligned with the first baseline; the second axis e_2 is perpendicular to

[¶]Throughout this work, a matrix for which the columns are orthogonal normal vectors is defined as an orthonormal matrix. In equivalent terms, an orthonormality constraint implies both the normality and orthogonality of the column vectors of a matrix.

the first, lying in the plane formed by the first two baselines; and the third body axis e_3 is directed so that $e_1e_2e_3$ forms a right-handed orthonormal frame. The baseline coordinates expressed in the body frame F are transformed into the coordinates in the reference frame $x_1x_2x_3$ (B) as $B = RF$, where the orthonormal ($R^TR = I$) matrix R links the two frames by means of a rigid rotation.

The elements of the rotation matrix and the local baseline coordinates are defined as [42]

$$\begin{aligned} m \geq 3\text{: } RF &= [r_1, r_2, r_3]\begin{bmatrix} f_{11} & f_{21} & f_{31} & \cdots & f_{m1} \\ 0 & f_{22} & f_{32} & \cdots & f_{m2} \\ 0 & 0 & f_{33} & \cdots & f_{m3} \end{bmatrix} \\ m = 2\text{: } RF &= [r_1, r_2]\begin{bmatrix} f_{11} & f_{21} \\ 0 & f_{22} \end{bmatrix} \\ m = 1\text{: } RF &= [r_1][f_{11}] \end{aligned} \tag{3}$$

Recall that m is the number of baselines. The ith column of R is denoted r_i, and the f_{ij} are the scalar entries of F. For notational convenience, the parameter p is used to indicate the number of columns in R: $p = m$ for $m < 3$, and $p = 3$ for $m \geq 3$. Note that for the case $m = p = 1$, model (2) formally coincides with the single-baseline-length-constrained ILS problem described and tested previously [40,41].

Model (2) can now be reformulated in terms of the unknown attitude matrix R as [42]

$$\begin{aligned} Y = AZ + GRF + \Xi; \qquad & D(\mathrm{vec}(Y)) = Q_{YY} \\ Z \in \mathbb{Z}^{n\times m}; \qquad & R \in \mathbb{O}^{3\times p} \end{aligned} \tag{4}$$

where the unknowns to be resolved are the nm integer-valued ambiguities of Z and the $3p$ entries of the orthonormal matrix R. Note that, due to the orthonormality constraint, only three (or two in the case of a single baseline) terms of R are independent.

Assuming the same V–C matrix Q_{yy} for all the single-baseline observations, the V–C matrix Q_{YY} is constructed as

$$Q_{YY} = P_m \otimes Q_{yy} = \begin{bmatrix} 1 & 0.5 & \cdots & 0.5 \\ 0.5 & 1 & \cdots & \vdots \\ & & \ddots & 0.5 \\ 0.5 & \cdots & 0.5 & 1 \end{bmatrix} \otimes Q_{yy} \tag{5}$$

where P_m takes care of the correlations among observations due to the common reference antenna used to form the DD observations.

3. Attitude Parameterization

The orthonormal rotation matrix R is parameterized with one of the different representations that can be employed for three-dimensional rotations, such as the Gibbs vector, the direct cosine matrix, the quaternions, and the Euler angles [50,51]. To visualize the attitude angles, a Euler parameterization (namely, a 321 configuration) is used in this contribution: the rotation matrix is expressed in terms of heading (ψ), elevation (θ), and bank (ϕ) angles as

$$R(\psi,\theta,\phi) = \begin{bmatrix} C_\psi C_\theta & C_\psi S_\theta S_\phi + S_\psi C_\phi & C_\psi S_\theta C_\phi - S_\psi S_\phi \\ -S_\psi C_\theta & -S_\psi S_\theta S_\phi + C_\psi C_\phi & -S_\psi S_\theta C_\phi - C_\psi S_\phi \\ -S_\theta & C_\theta S_\phi & C_\theta C_\phi \end{bmatrix} \tag{6}$$

where $C_\xi = \cos(\xi)$ and $S_\xi = \sin(\xi)$. In case $p < 3$, only the first p columns of R are considered. The advantage of this representation is that the orthonormality constraint is implicitly fulfilled. The disadvantage is that the evaluation of R and its derivatives requires the computation of trigonometric functions. Moreover, an ambiguity may arise, since matrix $R(\psi,\theta,\phi)$ is equivalently expressed with $R(\psi+\pi, \theta-\pi, \phi+\pi)$. This ambiguity is usually avoided by imposing $-\frac{\pi}{2} < \theta < \frac{\pi}{2}$. This parameterization employs a minimal set of parameters, as only three independent variables are used to describe the rotation matrix, and the number of degrees of freedom is exactly three.

The estimation of the orthonormal matrix R has a lower computational load when employing a quaternion parameterization, for which

$$\begin{aligned} R(\bar{q}) = R(q,q_4) &= (q_4^2 - \|q\|^2)I_3 + 2qq^T + 2q_4[q^+] \\ &= \begin{bmatrix} q_1^2-q_2^2-q_3^2+q_4^2 & 2(q_1q_2+q_3q_4) & 2(q_1q_3-q_2q_4) \\ 2(q_1q_2-q_3q_4) & -q_1^2+q_2^2-q_3^2+q_4^2 & 2(q_2q_3+q_1q_4) \\ 2(q_1q_3+q_2q_4) & 2(q_2q_3-q_1q_4) & -q_1^2-q_2^2+q_3^2+q_4^2 \end{bmatrix} \end{aligned} \tag{7}$$

where the quaternion $\bar{q} = (q, q_4)^T$ is partitioned by $q = (q_1, q_2, q_3)^T$, the vectorial part, and the scalar component q_4. The term $[q^+]$ equals the skew-symmetric matrix

$$[q^+] = \begin{bmatrix} 0 & q_3 & -q_2 \\ -q_3 & 0 & q_1 \\ q_2 & -q_1 & 0 \end{bmatrix} \tag{8}$$

The main advantage of the quaternion representation is that the first-order derivatives of the components of R are linear, and the second-order derivatives are constant: this proves to be an advantage for numerical schemes such as the Newton method. The shortcoming is that the orthonormality of R is only guaranteed for normal quaternions $\bar{q}^T\bar{q} = 1$, a constraint that has to be respected.

B. Least-Squares Solution

This subsection describes the rigorous least-squares solution to model (4). The solution is presented in three steps. First, the unconstrained least-squares solution of Eq. (4) is addressed:

$$\{\hat{Z}, \hat{R}\} = \arg \min_{Z\in\mathbb{R}^{n\times m}; R\in\mathbb{R}^{3\times p}} \|\mathrm{vec}(Y - AZ - GRF)\|^2_{Q_{YY}} \tag{9}$$

where the weighted norm of a given vector v is denoted as $\|v\|^2_Q = v^TQ^{-1}v$. The solution of Eq. (9) provides coarse values for the unknowns, which generally do not respect the given constraints.

Next, the unconstrained ILS theory is presented, which may be applied to estimate the integer ambiguities without considering the known geometrical constraints:

$$\{\check{Z}^U, \check{R}^U\} = \arg \min_{Z\in\mathbb{Z}^{n\times m}; R\in\mathbb{R}^{3\times p}} \|\mathrm{vec}(Y - AZ - GRF)\|^2_{Q_{YY}} \tag{10}$$

This formulation is given to allow for comparison with the constrained ILS theory illustrated in the following. The full solution of the constrained model (4), where both the integerness of the ambiguities and the orthonormality of R are respected, is given by

$$\{\check{Z}^C, \check{R}^C\} = \arg \min_{Z\in\mathbb{Z}^{n\times m}; R\in\mathbb{O}^{3\times p}} \|\mathrm{vec}(Y - AZ - GRF)\|^2_{Q_{YY}} \tag{11}$$

1. Unconstrained Least-Squares Solution

The unconstrained least-squares problem (9) is formulated by disregarding the integer nature of Z and the orthonormality of R. The float estimators $\hat{Z}$ and $\hat{R}$ are obtained by solving the normal equations

$$\begin{aligned} N\begin{pmatrix} \mathrm{vec}(\hat{Z}) \\ \mathrm{vec}(\hat{R}) \end{pmatrix} &= \begin{bmatrix} P_m^{-1} \otimes A^TQ_{yy}^{-1} \\ FP_m^{-1} \otimes G^TQ_{yy}^{-1} \end{bmatrix}\mathrm{vec}(Y) \\ N &= \begin{bmatrix} P_m^{-1} \otimes A^TQ_{yy}^{-1}A & P_m^{-1}F^T \otimes A^TQ_{yy}^{-1}G \\ FP_m^{-1} \otimes G^TQ_{yy}^{-1}A & FP_m^{-1}F^T \otimes G^TQ_{yy}^{-1}G \end{bmatrix} \end{aligned} \tag{12}$$

The derivation of the normal equations (12) follows from the properties of the vec operator and Kronecker product (see Appendix A). The V–C matrices of the float solutions are obtained by inversion of the normal matrix

$$\begin{bmatrix} Q_{\hat{Z}\hat{Z}} & Q_{\hat{Z}\hat{R}} \\ Q_{\hat{R}\hat{Z}} & Q_{\hat{R}\hat{R}} \end{bmatrix} = N^{-1} \tag{13}$$

The accuracy of the float solution is driven by the precision of the code observables, which then provide a coarse solution. This is demonstrated as follows. The design matrices A and G and V–C matrix Q_{yy} can be rewritten as

$$A = \begin{bmatrix} \lambda I_n \\ 0 \end{bmatrix} \qquad G = \begin{bmatrix} U \\ U \end{bmatrix} \qquad Q_{yy} = \begin{bmatrix} \sigma_\varphi^2 Q & 0 \\ 0 & \sigma_p^2 Q \end{bmatrix} \tag{14}$$

where λ is the carrier wavelength, U is the matrix of differenced unit line-of-sight vectors, Q is the covariance matrix that takes care of the correlation introduced by the DD operation, and σ_φ and σ_p are the phase and code standard deviations, respectively. The explicit computation of the matrix inverse in Eq. (13), exploiting the relations listed in Appendix B, gives

$$\begin{aligned} Q_{\hat{Z}\hat{Z}} &= P_m \otimes (A^T Q_{yy}^{-1} A)^{-1} + F^T (F P_m^{-1} F^T)^{-1} F \\ &\quad \otimes [(A^T Q_{yy}^{-1} A)^{-1} A^T Q_{yy}^{-1} G (\bar{G}^T Q_{yy}^{-1} \bar{G})^{-1} G^T Q_{yy}^{-1} A (A^T Q_{yy}^{-1} A)^{-1}] \\ &= \frac{\sigma_p^2}{\lambda^2} \left[P_m \otimes \frac{\sigma_\varphi^2}{\sigma_p^2} Q + F^T (F P_m^{-1} F^T)^{-1} F \otimes U (U^T Q^{-1} U)^{-1} U^T \right] \\ Q_{\hat{R}\hat{R}} &= (F P_m^{-1} F^T)^{-1} \otimes (\bar{G}^T Q_{yy}^{-1} \bar{G})^{-1} = (F P_m^{-1} F^T)^{-1} \\ &\quad \otimes \sigma_p^2 (U^T Q^{-1} U)^{-1} \end{aligned} \tag{15}$$

with $\bar{G} = [I - A(A^T Q_{yy}^{-1} A)^{-1} A^T Q_{yy}^{-1}] G$. Given the ratio $\sigma_\varphi^2 / \sigma_p^2 \approx 10^{-4}$, it is clear that the precision of float estimates $\hat{Z}$ and $\hat{R}$ is driven by the less precise code observables.

2. Sum-of-Squares Decomposition of Objective Function

The solutions of Eqs. (10) and (11) are obtained in the following by using a sum-of-squares decomposition of the objective function. The sum-of-squares decomposition of the squared norms in Eqs. (10) and (11) reads [45]

$$\begin{aligned} \|\mathrm{vec}(Y - AZ - GRF)\|_{Q_{YY}}^2 &= \|\mathrm{vec}(\hat{\Xi})\|_{Q_{YY}}^2 + \|\mathrm{vec}(\hat{Z} - Z)\|_{Q_{YY}}^2 \\ &\quad + \|\mathrm{vec}(\hat{R}(Z) - R)\|_{Q_{\hat{R}(Z)\hat{R}(Z)}}^2 \end{aligned} \tag{16}$$

The decomposition is based on the ambiguity float solution $\hat{Z}$ and the conditional attitude matrix $\hat{R}(Z)$, which is the (generally not orthonormal) attitude matrix obtained by considering the ambiguities Z as known. This means that $\hat{R}(Z)$ is derived as the least-squares solution of the model $E(Y - AZ) = GRF$, with $E(\cdot)$ as the expectation operator, which gives

$$\mathrm{vec}\,(\hat{R}(Z)) = \mathrm{vec}(\hat{R}) - Q_{\hat{R}\hat{Z}} Q_{\hat{Z}\hat{Z}}^{-1} \mathrm{vec}(\hat{Z} - Z) \tag{17}$$

The V–C matrix of $\hat{R}(Z)$ follows as

$$Q_{\hat{R}(Z)\hat{R}(Z)} = Q_{\hat{R}\hat{R}} - Q_{\hat{R}\hat{Z}} Q_{\hat{Z}\hat{Z}}^{-1} Q_{\hat{Z}\hat{R}} \tag{18}$$

Using the relations in Appendix B, the V–C matrix $Q_{\hat{R}(Z)\hat{R}(Z)}$ is written as

$$\begin{aligned} Q_{\hat{R}(Z)\hat{R}(Z)} &= (F P_m^{-1} F^T)^{-1} \otimes (G^T Q_{yy}^{-1} G)^{-1} \\ &= (F P_m^{-1} F^T)^{-1} \otimes \frac{\sigma_\varphi^2}{(\sigma_\varphi^2/\sigma_p^2) + 1} (U^T Q^{-1} U)^{-1} \\ &\approx (F P_m^{-1} F^T)^{-1} \otimes \sigma_\varphi^2 (U^T Q^{-1} U)^{-1} \end{aligned} \tag{19}$$

Hence, the precision of the conditional solution $\hat{R}(Z)$ is much higher than the precision of the float solution $\hat{R}$, as it depends on the accuracy of the phase observables.

3. Unconstrained Integer Least-Squares Solution

The unconstrained ILS problem (10) is formulated without taking into account the additional geometrical constraints. This is the problem often addressed for GNSS ambiguity resolution. The well-known ILS theory applies [27,36,52]. The ILS solution is derived following three steps. First, one obtains the float solution as Eq. (12). The second step is based on the sum-of-squares decomposition (16). For any choice of the matrix of ambiguities Z, the last term on the right-hand side of Eq. (16) can be made zero by selecting as attitude solution $R = \hat{R}(Z)$. Hence, minimizing Eq. (16) is equivalent to solving the multivariate ILS problem

$$\check{Z}^U = \arg \min_{Z \in \mathbb{Z}^{n \times m}} \|\mathrm{vec}(\hat{Z} - Z)\|_{Q_{\hat{Z}\hat{Z}}}^2 \tag{20}$$

The matrix of ambiguities $\check{Z}^U$ minimizes the distance with respect to the float solution $\hat{Z}$ in the metric defined by the V–C matrix $Q_{\hat{Z}\hat{Z}}$. As no analytical solutions of Eq. (20) are known, the matrix $\check{Z}^U$ is extensively searched in the set of admissible integer candidates

$$\Omega^U(\chi^2) = \{Z \in \mathbb{Z}^{n \times m} | \|\mathrm{vec}(\hat{Z} - Z)\|_{Q_{\hat{Z}\hat{Z}}}^2 \leq \chi^2\} \tag{21}$$

where the size of $\Omega^U(\chi^2)$ is defined by the scalar χ. Its value should be small enough to limit the computational burden, but the nonemptiness of $\Omega^U(\chi^2)$ should be guaranteed. By experience, a good choice is to make use of the bootstrapped value Z_b [53,54]:

$$\chi^2 = \|\mathrm{vec}(\hat{Z} - Z_b)\|_{Q_{\hat{Z}\hat{Z}}}^2 \tag{22}$$

The LAMBDA method is applied to perform the search for the minimizer $\check{Z}^U$: the ambiguities are decorrelated with an admissible transformation (i.e., which preserves the integerness of the variables), resulting in a much less elongated search space [28]. The minimizer $\check{Z}^U$ is then efficiently searched within the set $\Omega^U(\chi^2)$.

The last step for the solution of Eq. (10) is to extract the matrix $\check{R}^U$ as

$$\mathrm{vec}\,(\check{R}^U) = \mathrm{vec}(\hat{R}(\check{Z}^U)) = \mathrm{vec}(\hat{R}) - Q_{\hat{R}\hat{Z}} Q_{\hat{Z}\hat{Z}}^{-1} \mathrm{vec}(\hat{Z} - \check{Z}^U) \tag{23}$$

Note that the attitude solution $\check{R}^U$ is generally not orthonormal, but it may be a good enough approximation for many applications. If necessary, the closest orthonormal matrix to $\check{R}^U$ can be determined by means of one of the methods reviewed in Sec. II.C.

4. Constrained Integer Least-Squares Solution

The rigorous ILS solution of Eq. (4), satisfying the two constraints on the matrices of unknowns $Z \in \mathbb{Z}^{n \times m}$ and $R \in \mathbb{O}^{3 \times p}$, is now addressed. Aiming to minimize the weighted squared norm of residuals, the problem is formulated as in Eq. (11). The sum-of-squares decomposition (16) applies to Eq. (11). Because of the constraint on the attitude matrix, the last term on the right-hand side of Eq. (16) can no longer be made zero by choosing $R = \hat{R}(Z)$, since $\hat{R}(Z)$ is generally not orthonormal. Therefore, minimizing Eq. (11) is equivalent to minimizing the cost function $C(Z)$:

$$\begin{aligned} \check{Z}^C &= \arg \min_{Z \in \mathbb{Z}^{n \times m}} C(Z) \\ C(Z) &= \|\mathrm{vec}(\hat{Z} - Z)\|_{Q_{\hat{Z}\hat{Z}}}^2 + \|\mathrm{vec}(\hat{R}(Z) - \check{R}(Z))\|_{Q_{\hat{R}(Z)\hat{R}(Z)}}^2 \end{aligned} \tag{24}$$

with

$$\mathrm{vec}\,(\check{R}(Z)) = \arg \min_{R \in \mathbb{O}^{3 \times p}} \|\mathrm{vec}(\hat{R}(Z) - R)\|_{Q_{\hat{R}(Z)\hat{R}(Z)}}^2 \tag{25}$$

The cost function $C(Z)$ is the sum of two coupled terms. The first weighs the distance from the float ambiguity matrix $\hat{Z}$ to the nearest integer matrix Z in the metric of $Q_{\hat{Z}\hat{Z}}$, whereas the second weighs the distance from the conditional float solution $\hat{R}(Z)$ to the nearest orthonormal matrix $\check{R}(Z)$ in the metric of $Q_{\hat{R}(Z)\hat{R}(Z)}$. The integral resolution of both the ambiguities and the attitude matrix is the core of the new method: the search for the integer minimizer of Eq. (24) embeds the nonlinear geometrical constraints, resulting in a strengthened model. The method is a rigorous application of the nonlinearly constrained ILS principle, but a potential drawback is an increased numerical complexity. The search space is now

$$\Omega^C(\chi^2) = \{Z \in \mathbb{Z}^{n\times m} | C(Z) \leq \chi^2\} \tag{26}$$

Two issues make the search for the integer minimizer complex. First, the search space is not ellipsoidal as it was in the unconstrained case. Second, the choice of χ^2 is critical. The search for the minimizer of Eq. (24) implies the evaluation of Eq. (25) for each of the integer candidates in $\Omega^C(\chi^2)$, and a too-large value of χ^2 means that the constrained least-squares problem (25) has to be evaluated many times, increasing the computational load. As an example, Fig. 1 shows the value of χ^2 calculated from an integer bootstrapped matrix Z_b [as in Eq. (22)] for the flight test described in the next section. The scalar $\chi^2 = C(Z_b)$ is visualized and compared with the value $\chi_1^2 = \|\text{vec}(\hat{Z} - Z_b)\|^2_{Q_{\hat{z}\hat{z}}}$, which is the scalar that one obtains for the unconstrained approach: χ^2 is often four orders of magnitude larger than χ_1^2. The reason is that χ_1^2 is obtained by weighting the squared norm $\|\text{vec}(\hat{Z} - Z)\|^2$ with the inverse of the V–C matrix $Q_{\hat{Z}\hat{Z}}$, which has entries with a magnitude comparable to the code standard deviation, as in Eq. (15). Instead, the term $\|\text{vec}(\hat{R}(Z) - \check{R}(Z))\|^2$ in $C(Z)$ is weighted by the inverse of the V–C matrix $Q_{\hat{R}(Z)\hat{R}(Z)}$, for which the entries, according to Eq. (19), are driven by the carrier phase observables precision. It is shown in the next section that the MC-LAMBDA method overcomes this issue through the use of novel easy-to-evaluate bounding functions.

5. *Multivariate Constrained LAMBDA Method*

Following the previous discussion, it is clear that a numerical efficient search method has to overcome two issues: the initial size of the search space has to be properly set, and unnecessary evaluations of Eq. (25) should be avoided. This is accomplished by considering that the cost function $C(Z)$ can be bounded by two easier-to-evaluate functions [42]. Denoting the smallest and the largest eigenvalues of $Q^{-1}_{\hat{R}(Z)\hat{R}(Z)}$ with λ_m and λ_M, respectively, the following inequalities hold true:

$$C_1(Z) \leq C(Z) \leq C_2(Z)$$

$$C_1(Z) = \|\text{vec}(\hat{Z} - Z)\|^2_{Q_{\hat{z}\hat{z}}} + \lambda_m \sum_{i=1}^{p} (\|\hat{r}_i(Z)\| - 1)^2$$

$$C_2(Z) = \|\text{vec}(\hat{Z} - Z)\|^2_{Q_{\hat{z}\hat{z}}} + \lambda_M \sum_{i=1}^{p} (\|\hat{r}_i(Z)\| + 1)^2 \tag{27}$$

where $\hat{r}_i(Z)$ is the ith column of $\hat{R}(Z)$, and the inequalities are derived by applying the rules of the scalar product between vectors. The bounds $C_1(Z)$ and $C_2(Z)$ generate two search spaces that bound the one of $C(Z)$. For a given scalar χ, the set $\Omega_2(\chi^2)$ corresponding to the upper bound $C_2(Z)$ is contained in $\Omega^C(\chi^2)$, whereas the set $\Omega_1(\chi^2)$ corresponding to the lower bound $C_1(Z)$ contains $\Omega^C(\chi^2)$. Two search strategies have been devised to exploit these two bounds and perform the search for the integer minimizer in an efficient way: the search and shrink and the expansion approaches.

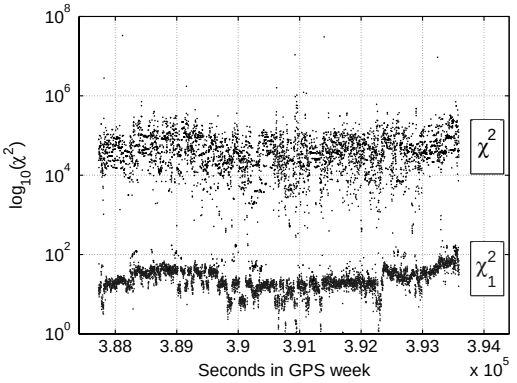

Fig. 1 Demonstration of large weight of second term in Eq. (24). Note the logarithmic scale of the χ^2 axis.

The search and shrink approach works with the upper bound $C_2(Z)$ and the related search space

$$\Omega_2(\chi_0^2) = \{Z \in \mathbb{Z}^{n\times m} | C_2(Z) \leq \chi_0^2\} \subseteq \Omega^C(\chi_0^2) \tag{28}$$

The value for χ_0 is chosen large enough to guarantee the nonemptiness of $\Omega_2(\chi_0^2)$ and $\Omega^C(\chi_0^2)$. An integer candidate in the set $\Omega_2(\chi_0^2)$ is searched, aiming to find a matrix Z_1 providing a smaller value for the upper bound $C_2(Z_1) = \chi_1^2 < \chi_0^2$. Once it is found, the set is shrunk to $\Omega_2(\chi_1^2)$ and the search continues by looking for another integer candidate Z_2 capable of reducing the value $C_2(Z_2) = \chi_2^2 < \chi_1^2$. This procedure iteratively proceeds until the minimizer of $C_2(Z)$, say $\check{Z}_2$, is found. Since this may differ from the minimizer of $C(Z)$, the search space $\Omega^C(\bar{\chi}^2)$, with $\bar{\chi}^2 = C_2(\check{Z}_2)$, is evaluated:

$$\Omega^C(\bar{\chi}^2) = \{Z \in \mathbb{Z}^{n\times m} | C(Z) \leq \bar{\chi}^2\} \supseteq \Omega_2(\bar{\chi}^2) \tag{29}$$

The sought-for minimizer $\check{Z}^C$ is then extracted among the candidates contained in $\Omega^C(\bar{\chi}^2)$.

The expansion approach works the other way around. Initially, a small value for the scalar χ_0 is chosen to set the size of the search space $\Omega_1(\chi_0^2)$:

$$\Omega_1(\chi_0^2) = \{Z \in \mathbb{Z}^{n\times m} | C_1(Z) \leq \chi_0^2\} \supseteq \Omega(\chi_0^2) \tag{30}$$

The choice for χ_0 does not necessarily assure the nonemptiness of the set. The scalar χ is iteratively increased until, at step s, the set $\Omega_1(\chi_s^2)$ is nonempty. All the integer candidates in $\Omega_1(\chi_s^2)$ are then enumerated, and the set $\Omega^C(\chi_s^2)$ is evaluated by computing the cost function $C(Z)$ for each of the enumerated matrices. If $\Omega^C(\chi_s^2)$ is nonempty, the minimizer $\check{Z}^C$ of $C(Z)$ is picked up. Otherwise, the scalar $\chi_{s+1} > \chi_s$ is increased and the enumeration in the larger $\Omega_1(\chi_{s+1}^2)$ is repeated until, at step $s + k$, the set $\Omega^C(\chi_{s+k}^2)$ turns out to be nonempty.

Employing one of these two search algorithms reduces the computational burden, as the cost function (24) is now evaluated for a smaller set of integer candidates, whereas the main part of the search is performed through the use of $C_1(Z)$ and $C_2(Z)$, for which the resolution of Eq. (25) is not necessary. The efficiency of the alternative search strategies depends on the tightness of the bounds: the better the bounds approximate the cost function, the smaller the number of integer candidates for which the evaluation of Eq. (25) is necessary to extract the final global minimizer. The search and shrink approach has the advantage of self-adapting the size of the search space as the search proceeds, whereas the expansion approach makes use of an a priori value for the increment of the scalar χ. It has been shown that both techniques have comparable performance in terms of computational times, largely reducing the computational burden with respect to an exhaustive search [26,55]. Computational times suitable for real-time use have been registered.** Sharper boundaries for the objective function could further reduce the time needed to extract the integer minimizer.

C. Attitude Estimation

The evaluation of the cost function $C(Z)$ in Eq. (24) involves the computation of the constrained least-squares problem (25). Also, the solution of the unconstrained ILS problem $\hat{R}(\check{Z}^U)$ in Eq. (23) is generally not orthonormal, and one may want to determine the closest orthonormal matrix.

In both cases, the problem is to find the closest orthonormal matrix to a given matrix $\hat{R}_Z$, which can be formulated as

$$\check{R} = \arg \min_{R \in \mathbb{O}^{3\times p}} \|\text{vec}(\hat{R}_Z - R)\|^2_Q \tag{31}$$

This problem differs from the well-known problem of estimating the attitude from a set of baseline observations [56], mainly due to the shape of the weight matrix Q. If Q were a scaled unit matrix, $Q = \mu I$, expression (31) could be reformulated as an orthogonal Procrustes

**MATLAB implementation, nonoptimized code.

problem, or Wahba's problem [57], for which the analytical solution exists [57–59]. Several efficient numerical algorithms have been devised to quickly determine the orthonormal attitude matrix, such as the quaternion estimator [60,61], the fast optimal attitude matrix [62], the estimator of the optimal quaternion (ESOQ) [63] or the second ESOQ [64] algorithms. These algorithms have been extensively compared [65–67].

Unfortunately, the V–C matrix Q for GNSS-based attitude estimation [see Eq. (18)] is generally fully populated, implying that the previous approaches cannot be applied. Therefore, the orthonormal attitude matrix has to be numerically extracted by solving problem (31), for which three schemes are briefly reviewed in the following.

1. Solution Based on Lagrangian Multipliers Method

A first numerical scheme is derived by applying the Lagrangian multipliers method. It comprises finding the stationary points of the Lagrangian function [68]

$$L(R,[\mu]_p) = \mathrm{vec}(\hat{R}_Z - R)^T Q^{-1}\mathrm{vec}(\hat{R}_Z - R) - \mathrm{tr}([\mu]_p[R^TR - I_p]) \tag{32}$$

where tr indicate the trace of a matrix, and $[\mu]_p$ is the $p \times p$ symmetric matrix of Lagrangian multipliers. The last term of Eq. (32) gives the $[p(p+1)]/2$ constraining functions that follow from the orthonormality of R: p constraints arise from the normality of the columns of R, and $[p(p-1)]/2$ constraints originate from the orthogonality of the columns of R. The gradient of the Lagrangian function (32), together with the $[p(p+1)]/2$ constraining functions, defines the nonlinear system to be solved:

$$\begin{cases} \frac{1}{2}\nabla L(R,[\mu]_p) = (Q^{-1} - [\mu]_p \otimes I_3)\mathrm{vec}(R) - Q^{-1}\mathrm{vec}(\hat{R}_Z) = 0 \\ \mathrm{vec}(R^TR - I_p) = 0 \end{cases} \tag{33}$$

Because of the symmetry of the matrix $[R^TR - I_p]$, only its upper (or lower) triangular part has to be considered in the second set of equations in Eq. (33). The Newton–Raphson method is applied to iteratively converge to the sought orthonormal matrix of rotations.

This method is computationally heavier than other iterative schemes, as it requires the explicit evaluation of large matrices and it does not use a minimal set of variables. For these reasons, this approach can be twice as slow compared with both methods presented in the following.

2. Solution Based on Euler Angles Parameterization

After reparameterizing the attitude matrix in terms of the vector of Euler angles $\eta = (\psi, \theta, \phi)^T$, the matrix $R(\eta)$ implicitly fulfills the constraint $R^TR = I_p$, and problem (31) is rewritten as

$$\check{\eta} = \arg\min_{\eta\in\mathbb{R}^3} \|h(\eta)\|_I^2 = \arg\min_{\eta\in\mathbb{R}^3} h(\eta)^T h(\eta) \tag{34}$$

with $h(\eta) = Q^{-\frac{1}{2}}\mathrm{vec}(\hat{R}_Z - R(\eta))$ as the vector of $3p$ nonlinear functions of η. The nonlinear least-squares problem (34) can be solved by means of the Gauss–Newton method or the Newton method. The Gauss–Newton method is the simplest of the two methods. It has a local linear rate of convergence, and it only requires first-order partial derivatives of $h(\eta)$. The method works well in case of moderate curvatures and small residuals [69]. The Newton method is an improved alternative, which has a local quadratic rate of convergence, but it requires second-order partial derivatives as well.

The Euler angles parameterization approach has the advantage of working with a minimal set of unknowns (the Euler angles), and it can quickly converge to the sought minimizer if an accurate initial guess is used. The disadvantage is that trigonometric functions have to be evaluated, increasing the computational load.

3. Solution Based on Quaternions Parameterization

Quaternions can be used to reparameterize the rotation matrix R and solve for Eq. (31):

$$\check{\bar{q}} = \arg\min_{\bar{q}\in\mathbb{R}^4, \|\bar{q}\|=1} \|\mathrm{vec}(\hat{R}_Z - R(\bar{q}))\|_Q^2 \tag{35}$$

The orthonormality constraint for R is guaranteed by the normality of the quaternion: this introduces the constraint $\|\bar{q}\| = 1$ in the minimization problem (35). A Lagrangian function is formed as

$$L'(\bar{q},\mu') = \mathrm{vec}(\hat{R}_Z - R(\bar{q}))^T Q^{-1}\mathrm{vec}(\hat{R}_Z - R(\bar{q})) - \mu'(\bar{q}^T\bar{q} - 1) \tag{36}$$

with μ' as the Lagrangian parameter. The (nonlinear) system to be solved is

$$\begin{cases} \frac{1}{2}\nabla L'(\bar{q},\mu') = J_{R(\bar{q})}^T Q^{-1}\mathrm{vec}(\hat{R}_Z - R(\bar{q})) - \mu'\bar{q} = 0 \\ \bar{q}^T\bar{q} - 1 = 0 \end{cases} \tag{37}$$

with $J_{R(\bar{q})}$ as the Jacobian of $\mathrm{vec}(R(\bar{q}))$.

Table 1 Step-by-step overview of the proposed methods for GNSS carrier phase attitude estimation

Form the design matrices
A, G, F
↓
Form the DD matrices of observables and covariance
Y, Q_{YY}
↓
Float estimation
$$\begin{pmatrix} \mathrm{vec}(\hat{Z}) \\ \mathrm{vec}(\hat{R}) \end{pmatrix} = N^{-1}\begin{bmatrix} P_m^{-1} \otimes A^T Q_{yy}^{-1} \\ FP_m^{-1} \otimes G^T Q_{yy}^{-1} \end{bmatrix}\mathrm{vec}(Y)$$
↓
Search for the integer minimizer

LAMBDA	MC-LAMBDA
$\check{Z}^U = \arg\min_{Z\in\mathbb{Z}^{n\times m}} \|\mathrm{vec}(\hat{Z} - Z)\|_{Q_{\hat{z}\hat{z}}}^2$	$\check{Z}^C = \arg\min_{Z\in\mathbb{Z}^{n\times m}} C(Z)$
	$C(Z) = \|\mathrm{vec}(\hat{Z} - Z)\|_{Q_{\hat{z}\hat{z}}}^2 + \|\mathrm{vec}(\hat{R}(Z) - \check{R}(Z))\|_{Q_{\hat{R}(Z)\hat{R}(Z)}}^2$
	↓
	Search and shrink/expansion
↓	↓
Attitude estimation	
$\check{R}(\check{Z}^U) = \arg\min_{R\in\mathbb{O}^{3\times p}} \|\mathrm{vec}(\hat{R}(\check{Z}^U) - R)\|_{Q_{\hat{R}(Z)\hat{R}(Z)}}^2$	$\check{R}(\check{Z}^C) = \arg\min_{R\in\mathbb{O}^{3\times p}} \|\mathrm{vec}(\hat{R}(\check{Z}^C) - R)\|_{Q_{\hat{R}(Z)\hat{R}(Z)}}^2$

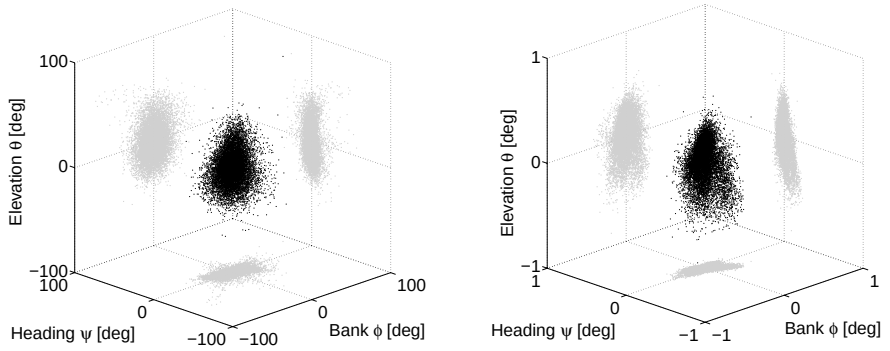

a) Attitude angles: float solution **b) Attitude angles: fixed solution**

Fig. 2 Three estimated Euler angles for a three-antenna configuration of (both) 2-m-long baselines derived with the float estimator (left) and the fixed (ambiguities correctly resolved) estimator (right). Precision differs by two orders of magnitude.

This approach guarantees the best tradeoff, as it makes use of a small number of unknowns, no trigonometric functions have to be evaluated, and the first-order derivatives in $J_{R(\bar{q})}$ are linear functions of the unknowns.

4. Initialization of Numerical Schemes

The three numerical schemes described above make use of an initial guess for the vector of unknowns. A good choice is to first compute an orthonormal matrix $\bar{R}$ by solving Eq. (31) under the assumption that Q is an identity matrix, so that Eq. (31) reduces to the Whaba problem, and an analytical solution exists [57–59]. Then, the initialization vectors for each of the three numerical schemes read

$$\begin{aligned} &\text{Lagrangian multipliers}: \gamma^0 = [x_1^0, \ldots, x_{3p}^0, 0, \ldots, 0]^T \\ &\text{Euler angles parameterization}: \eta^0 = [\psi^0, \theta^0, \phi^0]^T \\ &\text{Quaternions parameterization}: \omega^0 = [\bar{q}^0, 0]^T \end{aligned} \tag{38}$$

with x_i^0 as the ith entry of $\text{vec}(\bar{R})$, $(\psi^0, \theta^0, \phi^0)$ as the Euler angles parameterization of $\text{vec}(\bar{R})$, and $\bar{q}^0$ as the quaternions parameterization of $\text{vec}(\bar{R})$. The Lagrangian parameters in the first and last methods in Eq. (38) are all initially set to zero, following the assumption that the initial coarse solution is sufficiently close to an orthonormal matrix.

5. Schematic Overview

Table 1 gives an overview of the various computational steps that have been reviewed so far. Both the unconstrained and constrained methods are listed. The difference in the achieved accuracy between the attitude float estimation $\hat{R}$ and an estimate made considering the ambiguities as known, $\breve{R}(Z)$, is visualized in Fig. 2. The attitude angles for two static (2 m long) baselines are determined using the two estimators. Obviously, a two-order-of-magnitude improvement is obtained when the ambiguities are resolved as integers.

III. Simulations

A reliable testing of the new method performance is obtained by means of simulations. Series of simulated data sets are generated via a Monte Carlo approach, with a predefined type and amount of error. The theoretical SE–SF success rate is investigated as a function of the model strength; that is, it is examined how the success rate varies with respect to the number of available observations and noise levels. The results obtained by applying the MC-LAMBDA method are compared with respect to the classical ILS approach (LAMBDA method). Observations from five to eight satellites are simulated according to model (4). Simulation parameters are reported in Appendix C. White noise is introduced on the observations, ranging between 5 and 30 cm for the code measurements and between 3 and 30 mm for the carrier phase observations. Although the value of 30 mm for the carrier phase signal noise might seem unnecessary large, it is useful in order to investigate the limits of the proposed algorithm.

A first set of simulation results is given in Table 2, where the theoretical SE–SF success rate obtained on a single-baseline scenario is reported as a function of the model strength. The MC-LAMBDA method clearly provides better results than the unconstrained method. The differences in success rate are particularly pronounced when the underlying GNSS model becomes weaker (fewer satellites and/or higher measurement noise). Making use of the geometrical constraint (in the single-baseline case, this is a single constraint) improves the success rate considerably. According to Table 2, already five satellites and a phase standard deviation of 3 mm give a higher than 70% success rate. The differences in success rate become less pronounced when the strength of the underlying GNSS model increases. For instance, with eight satellites and a phase and code

Table 2 Simulation results: single-baseline SE–SF success rates (%) for LAMBDA and MC-LAMBDA methods per number of satellites, code, and phase noise levels[a]

		σ_Φ, *mm*								
		30			3			1		
		σ_P, *cm*								
	No. SV[b]	30	15	5	30	15	5	30	15	5
LAMBDA	5	0.41	2.84	29.59	3.30	19.50	86.67	5.99	26.89	95.37
MC-LAMBDA	5	3.47	9.57	41.64	72.43	88.86	99.63	96.54	99.94	100
LAMBDA	6	0.64	3.54	30.95	24.83	66.71	96.89	49.13	86.67	99.99
MC-LAMBDA	6	4.31	12.17	43.51	95.75	99.18	99.90	99.99	100	100
LAMBDA	7	0.83	4.40	34.08	50.24	79.69	99.53	74.17	93.27	100
MC-LAMBDA	7	5.80	14.41	46.34	99.34	99.97	100	100	100	100
LAMBDA	8	1.09	5.68	36.10	86.17	94.48	99.99	99.97	99.99	100
MC-LAMBDA	8	6.78	17.13	47.75	99.80	99.99	100	100	100	100

[a]10^5 data samples simulated.
[b]SV denotes space vehicle.

Table 3 Simulation results: two-baseline SE–SF success rates (%) for the LAMBDA and MC-LAMBDA methods, per number of satellites, code, and phase noise levels[a]

	σ_Φ, *mm*								
	30			3			1		
	σ_P, *cm*								
	30	15	5	30	15	5	30	15	5
5 LAMBDA	0.01	0.13	13.07	0.17	5.69	83.87	0.55	10.18	95.48
5 MC-LAMBDA	2.82	6.53	35.90	99.60	99.94	100	100	100	100
6 LAMBDA	0.01	0.21	15.26	9.81	56.89	96.83	30.12	81.35	100
6 MC-LAMBDA	2.35	6.81	38.90	99.99	100	100	100	100	100
7 LAMBDA	0.02	0.38	19.21	31.97	73.07	99.74	61.16	91.33	100
7 MC-LAMBDA	2.80	12.80	42.50	99.99	100	100	100	100	100
8 LAMBDA	0.03	0.67	21.90	81.72	93.12	99.99	99.99	100	100
8 MC-LAMBDA	4.50	13.90	45.50	100	100	100	100	100	100

[a]10^5 data samples simulated.

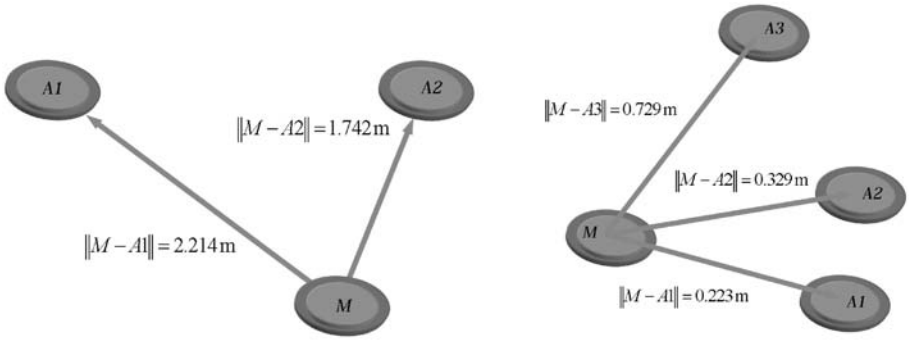

a) First static test: geometry of the two baselines (location: The Netherlands)

b) Second static test: geometry of the three baselines (location: Western Australia)

Fig. 3 Two static tests: geometrical arrangement of antennas.

precision of 3 mm and 5 cm, respectively, a close to 100% success rate is already achieved with the standard LAMBDA method.

Table 3 shows the SE–SF success rates for a two-baseline configuration. Also, in this case, the improvement is large especially for the weaker scenarios (lower number of satellite/higher noise levels), where the difference between the methods is significant. For example, with five satellites and 3 mm phase noise, the success rate increases from a low 0.17 to 99.60% when poor code measurements are simulated (30 cm). The two-baseline processing marks success rates higher than 99% on all the data sets processed with phase noise lower than 30 mm, obtaining a 100% success rate on 20 out of 24 simulated scenarios. As expected, the strengthening of the underlying model due to the embedded geometrical constraints substantially affects the capacity of fixing the correct integer ambiguity matrices.

IV. Experimental Testing: Static Configurations

The MC-LAMBDA method is first experimentally tested with data collected on two static frames of antennas: one in The Netherlands and one in Western Australia. The focus is on investigating the capacity of resolving the integer ambiguities on all the available baselines without any external aid, filtering, or dynamic modeling. No a priori information about the attitude is used, and no mask angles and elevation-dependent models are applied.

All the data sets processed have been analyzed offline. By postprocessing data (and not only looking at SE–SF results), the correct set of integers at each epoch could always be reconstructed. This offline processing is then used to assess the performance reported.

A. Static Test I

Three antennas (a Trimble Zephyr Geodetic L1/L2 as the master, and two geodetic Trimbles with ground planes as auxiliaries) were mounted on top of a rigid wooden structure of known geometry (see

Table 4 First static test: unaided SE–SF success rates (%) for the LAMBDA and MC-LAMBDA methods

Baseline	No. SV[a]	LAMBDA	MC-LAMBDA
	Single-baseline SE–SF success rate, %		
M-A1	4	1.6	44.3
	5	8.9	79.3
	6	42.0	98.2
	7	75.5	99.7
	8	97.4	100
	9	99.8	100
M-A2	4	0.8	49.1
	5	8.9	74.6
	6	40.1	97.1
	7	76.0	99.8
	8	96.9	100
	9	99.7	100
	Two-baseline SE–SF success rate, %		
M-A1-A2	4	0.9	84.2
	5	5.0	99.6
	6	38.9	100
	7	78.5	100
	8	97.7	100
	9	99.8	100

[a]SV denotes space vehicle.

Table 5 Second static test: configuration of GPS satellites used[a]

No. SV	PRNs	PDOP (average)
4 (a)	11-17-20-31	3.4
4 (b)	11-23-31-32	8.1
5 (a)	11-17-20-23-31	3.2
5 (b)	11-20-23-31-32	7.6
6	11-17-20-23-31-32	2.9
7	11-13-17-20-23-31-32	2.3

[a]PDOP values for the different configurations are reported.

Table 6 Second static test: unaided SE–SF success rates (%) for LAMBDA and MC-LAMBDA methods

Baseline	No. SV	LAMBDA	MC-LAMBDA
	Single-baseline SE–SF success rate, %		
M-A1	4 (a)	0.5	64.9
	4 (b)	0.7	87.2
	5 (a)	3.6	91.8
	5 (b)	3.2	100
	6	31.8	100
	7	60.5	100
M-A2	4 (a)	0.7	53.5
	4 (b)	0.5	97.3
	5 (a)	7.3	99.4
	5 (b)	14.6	99.9
	6	40.7	100
	7	60.9	100
M-A3	4 (a)	0.8	47.4
	4 (b)	0.6	66.1
	5 (a)	4.3	83.6
	5 (b)	11.4	94.7
	6	33.8	99.3
	7	70.3	100
	Two-baseline SE–SF success rate, %		
M-A1-A2	4 (a)	0.4	90.4
	4 (b)	0.1	97.9
	5 (a)	3.5	100
	5 (b)	3.0	100
	6	31.6	100
	7	65.9	100
M-A1-A3	4 (a)	0.5	99.9
	4 (b)	0.5	98.7
	5 (a)	3.0	99.9
	5 (b)	3.0	100
	6	31.1	100
	7	64.7	100
M-A3-A2	4 (a)	0.1	94.8
	4 (b)	0.5	87.7
	5 (a)	4.3	100
	5 (b)	11.5	99.8
	6	33.2	100
	7	74.8	100

Table 7 Second static test: mean and standard deviations of estimated attitude angles

		Heading ψ	Elevation θ	Bank ϕ
M-A1-A2	Mean, deg	89.2	1.9	0.3
	σ, deg	0.42	1.33	1.12
M-A1-A3	Mean, deg	89.3	1.9	0.3
	σ, deg	0.16	1.42	0.42
M-A3-A2	Mean, deg	6.1	0.09	1.5
	σ, deg	0.22	0.48	1.56

Table 8 First boat test: unaided SE–SF success rates (%) for LAMBDA and MC-LAMBDA methods[a]

Baseline	No. SV	LAMBDA	MC-LAMBDA
	Single-baseline SE–SF success rate, %		
1–2	Overall	82.0	99.5
	6	28.3	97.8
	7	81.2	99.8
	8	96.7	99.9
1–3	Overall	61.73	97.7
	6	8.8	84.6
	7	54.7	98.7
	8	83.5	99.8
	Two-baseline SE–SF success rate, %		
1-2-3	Overall	57.4	99.9
	6	14.8	99.7
	7	46.6	100
	8	80.9	100

[a]Success rate as function of satellites tracked is also reported.

Fig. 3a). The antennas were connected to three Trimble receivers (a Trimble R7 and two Trimble SSi). Data (1 Hz) were collected for almost 3 h, resulting in 9915 epochs. Table 4 reports the unaided SE–SF success rate obtained as a function of the number of satellites tracked and baselines embedded in the model. The number of satellites is artificially reduced in order to test the robustness of the methods against the constellation availability. Also, different numbers of baselines have been included in the model. For the single-baseline case, only the length is used as a priori constraint with the MC-LAMBDA method, whereas for the two-baseline case, the baseline lengths and the relative orientation between the baselines are all exploited as geometrical constraints. For the worst-case scenario (namely, only four satellites in view), already one constrained baseline is sufficient to increase the success rate from about 1% to about 44–49%. The SE–SF success rate is sensitive to the strength of the underlying model: including more baselines results in a significant improvement in the success rate for the constrained method due to the higher number of geometrical constraints. Embedding both baselines into a single model and exploiting the full set of constraints enhances the probability of correct fixing to about 84%, whereas the performance of the unconstrained LAMBDA method for the two-baseline case remains approximately unchanged. With more than four visible satellites, the success rate is always above 99% with the MC-LAMBDA method, and only a few additional epochs would be necessary to obtain a 100% success rate. A benefit of the constrained method is that it guarantees high robustness against those scenarios where the geometry of the GNSS constellation is poor.

The attitude solution provides an indication of the accuracy obtainable. In this case, the three attitude angles are characterized by standard deviations equal to $\sigma_\psi = 0.054°$ for the heading, $\sigma_\theta = 0.120°$ for the elevation, and $\sigma_\phi = 0.174°$ for the bank angle. The higher precision of the heading angle is due to the intrinsic characteristic of the GNSS working principle: the satellites cover, with respect to the receiver, only a hemisphere, causing higher dilution of precision in the vertical plane than in the horizontal plane.

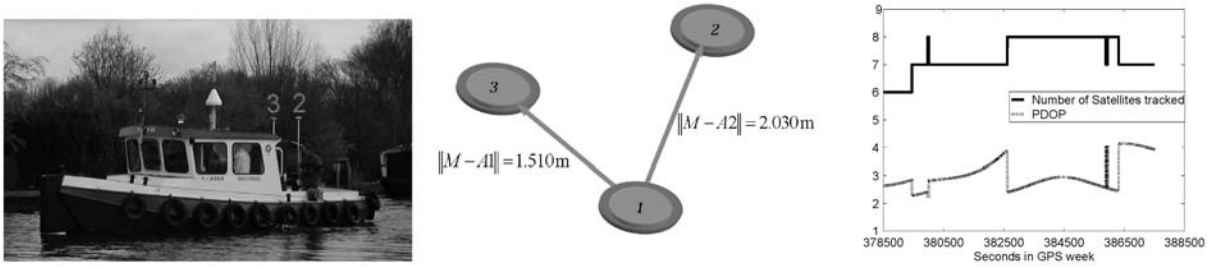

a) Boat with three antennas installed **b) Baselines formed by antennas installed aboard** **c) Number of tracked satellites and PDOP values**

Fig. 4 First boat test: three antennas/receivers mounted aboard a small vessel sailing along a canal in Delft, The Netherlands.

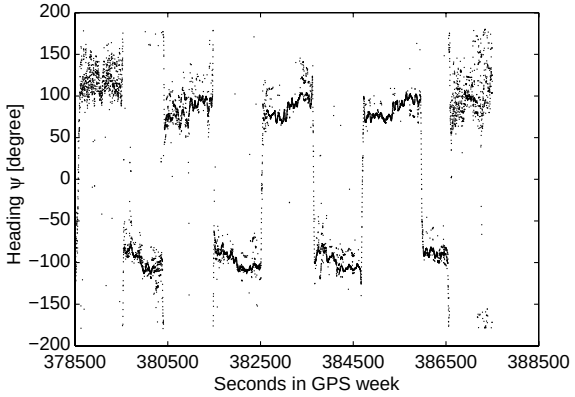

a) Heading $\psi(t)$, LAMBDA

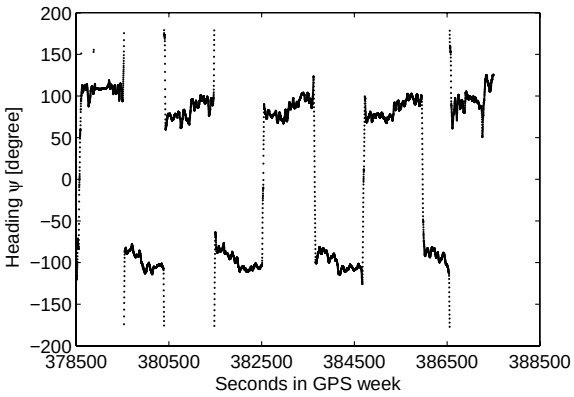

b) Heading $\psi(t)$, MC-LAMBDA

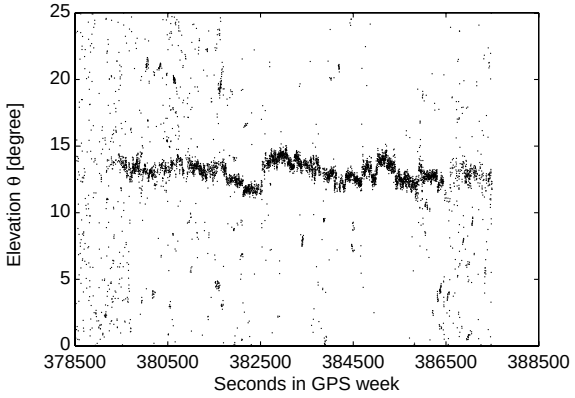

c) Elevation $\theta(t)$, LAMBDA

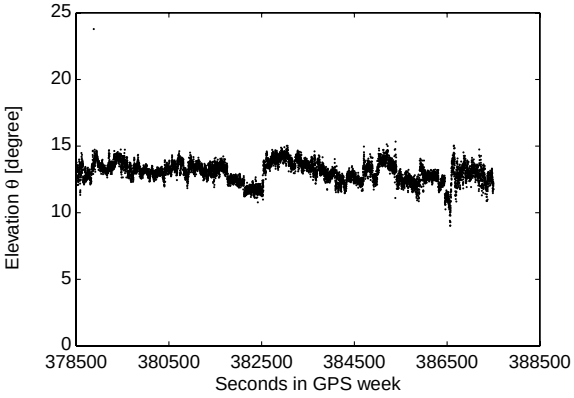

d) Elevation $\theta(t)$, MC-LAMBDA

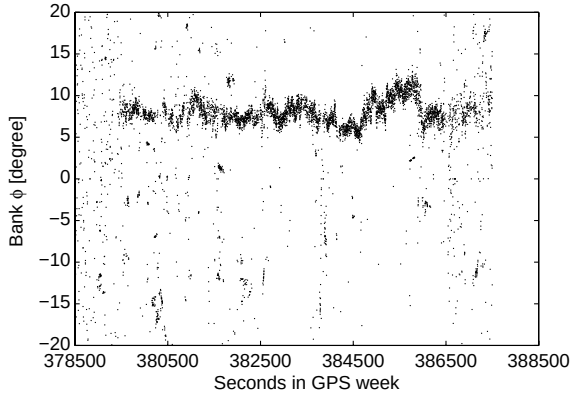

e) Bank $\phi(t)$, LAMBDA

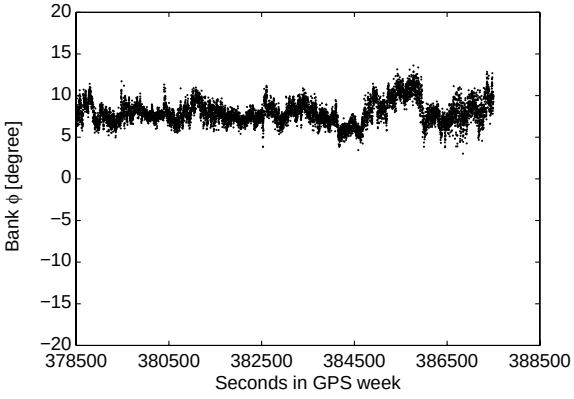

f) Bank $\phi(t)$, MC-LAMBDA

Fig. 5 First boat test: single-epoch full attitude solution, LAMBDA (left) vs MC-LAMBDA (right) method. Attitude is displayed as obtained epoch by epoch, without attempting any validation.

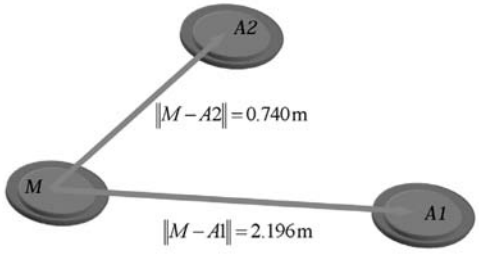

a) Relative geometry of the three antennas placed on top of the boat cabin

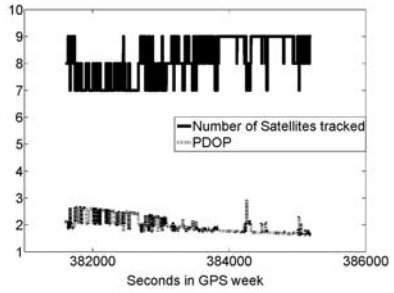

b) Number of tracked satellites and PDOP values

Fig. 6 Second boat test: three antennas/one receiver carried aboard a small vessel sailing along a canal in Delft, The Netherlands.

Table 9 Second boat test: unaided SE–SF success rates for LAMBDA and MC-LAMBDA methods[a]

Baseline	No. SV	LAMBDA	MC-LAMBDA
	Single-baseline SE–SF success rate, %		
	Overall	33.2	87.7
1–2	7	10.5	72.9
	8	26.3	85.0
	9	49.1	96.6
	Overall	40.7	95.6
1–3	7	19.5	93.5
	8	32.6	95.5
	9	49.5	96.2
	Two-baseline SE–SF success rate, %		
1-2-3	Overall	22.1	99.6
	7	3.2	99.7
	8	15.4	99.7
	9	37.7	99.3

[a]Success rate as function of satellites tracked is also reported.

B. Static Test II

A second static experiment was conducted at the Curtin University of Technology campus in Perth, Western Australia. Four Global Positioning System (GPS)-global navigation satellite system (GLONASS) receivers/antennas GSR 2700 ISX were placed on top of tripods at known distances (see Fig. 3b). Each of the receivers tracked, at most, seven satellites during a time span of about 20 min. Only GPS observations at single frequency L1 are processed. First, the three baselines are independently processed, attempting to fix the ambiguities on each of the baselines $M-A1$, $M-A2$, and $M-A3$. In these cases, only the baseline length is used as a priori information. Then, various two-baseline configurations ($M-A1-A2$, $M-A1-A3$, and $M-A3-A2$) have been considered, where the full set of constraints are exploited as geometrical constraints in the MC-LAMBDA method. In all the cases, one to three tracked satellites are artificially eliminated in order to test the performance as a function of the number of available satellites. For the four- and five-satellite scenarios, different combinations of satellites are used, as reported in Table 5, to test whether the geometry of the constellation somehow influences the results.

Table 6 reports the unaided SE–SF success rates obtained, processing the different data sets. The performance of the classical LAMBDA method largely depends on the number of satellites: success rates above 60% are only achieved with seven or more tracked satellites. Obviously, a large improvement is achieved with the MC-LAMBDA method. Already with a single-baseline processing, the success rate improves up to 100% on some of the data sets. As for the two-baseline configurations, the multivariate constrained method marks success rates higher than 99% on most of the data sets, notably also in one of the four-satellite scenarios where the standard method fails almost every epoch. When all three baselines are processed with the multivariate model, a 100% success rate is always achieved (not reported in Table 6). Noteworthy is that the MC-LAMBDA applied to two-baseline configurations often guarantees success rates higher than 90%, except for one data set. Note, however, that the impact of the GNSS constellation geometry cannot be directly inferred from this test alone.

The accuracy of the attitude solutions is provided in Table 7. The estimation error is higher than with the first static test due to the shorter baselines (see Fig. 3). Table 7 also highlights the relation between the attitude estimation precision and the baseline geometry employed: as expected, the longest baseline formed by the main and auxiliary (Aux3) antennas generally provides better angular accuracies.

V. Experimental Testing: Dynamic Platforms

This section present the evaluation of the MC-LAMBDA method based on three dynamic tests. The dynamic experiments were designed to test the method in the most challenging conditions: SE–SF processing of GPS-L1 data, where no a priori information about the attitude or the motion is provided, and mask angles, elevation-dependent models, dynamic models or any kind of filtering are not applied. Two low-dynamic experiments were carried out, collecting data on a slowly moving boat, whereas a flying aircraft provided the high-dynamic testing platform.

A. Boat Test I

The first data set processed was collected on a boat sailing the Schie canal in Delft, The Netherlands. The vessel was equipped with three antenna-receiver couples (see Fig. 4): 1) a choke-ring antenna connected to an Ashtech receiver; 2) an antenna connected to a Leica SR530 receiver; and 3) an antenna connected to a Novatel OEM3 receiver. The vessel sailed for about 2.5 h, collecting 9000 epochs of GPS observations. The number of tracked GPS satellites and position dilution of precision (PDOP) values are reported in Fig. 4. Table 8 reports the unaided SE–SF success rates obtained, both overall and per number of tracked satellites (between six and eight). Application of the MC-LAMBDA method results in a striking improvement, both in the single-baseline and in the two-baseline cases. Similar to the static experiments, the constrained method is much more robust with respect to variations in the number of available observations. Note that the success rates for the second baseline (1–3) are lower than those for the first baseline (1–2) when employing the LAMBDA method. This is due to the lower grade receiver, which yields poorer performance. Even more interesting, the MC-LAMBDA method is also capable of compensating the reduced quality of the observations by strengthening the underlying model.

Figure 5 shows the attitude angles obtained by estimating the rotation matrix epoch by epoch, without any attempt to validate the solution and taking the integer ambiguities as they are fixed with the LAMBDA or the MC-LAMBDA method (applied to the two-baseline case). The first method leads to a rather scattered plot, due to the low success rate (57.4%), resulting in many wrong ambiguity solutions, and hence less precise attitude solutions. In contrast, the constrained method provides a precise attitude solution more than 99% of the time.

B. Boat Test II

The second boat test took place on the same canal as the previous test. The same boat of Fig. 4a was equipped with a Septentrio PolaRx2 connected to three antennas AT502, for which the relative placement is visualized in Fig. 6a. The receiver collected GPS-L1 data for a total of 7200 epochs (2 Hz sampling). Figure 6b reports the number of tracked satellites with corresponding PDOP values. Table 9 shows the unaided SE–SF success rate for the classical and the constrained LAMBDA methods. The overall results, as well as the success rate per number of tracked satellites, are reported. As for the previous boat test, the improvement is rather large. The MC-LAMBDA method marks very high success rates in all cases.

Figure 7 compares the single-epoch attitude solutions as provided by the two algorithms: the benefit of having a reliable ambiguity resolution method is obvious.

C. Flight Test

A high-dynamic test was performed, processing data collected aboard the Cessna Citation II PH-LAB (see Fig. 8). This aircraft is equipped with different test systems and facilities, including several GPS antennas. Onboard the aircraft, a Septentrio PolaRx2 receiver was installed and connected to three antennas: an AIL DM-C L1-L2 placed on the middle of the fuselage and two L1/L2 Sensor Systems, one at the extremity of the left wing and one on the nose. Figure 8 shows the placement of the antennas. The matrix of local baseline coordinates for this antenna configuration is

$$F = \begin{bmatrix} 4.90 & -0.39 \\ 0 & 7.60 \end{bmatrix} \text{m} \tag{39}$$

The data set examined was collected during an airborne remote sensing campaign: the Gravimetry Using Airborne Inertial

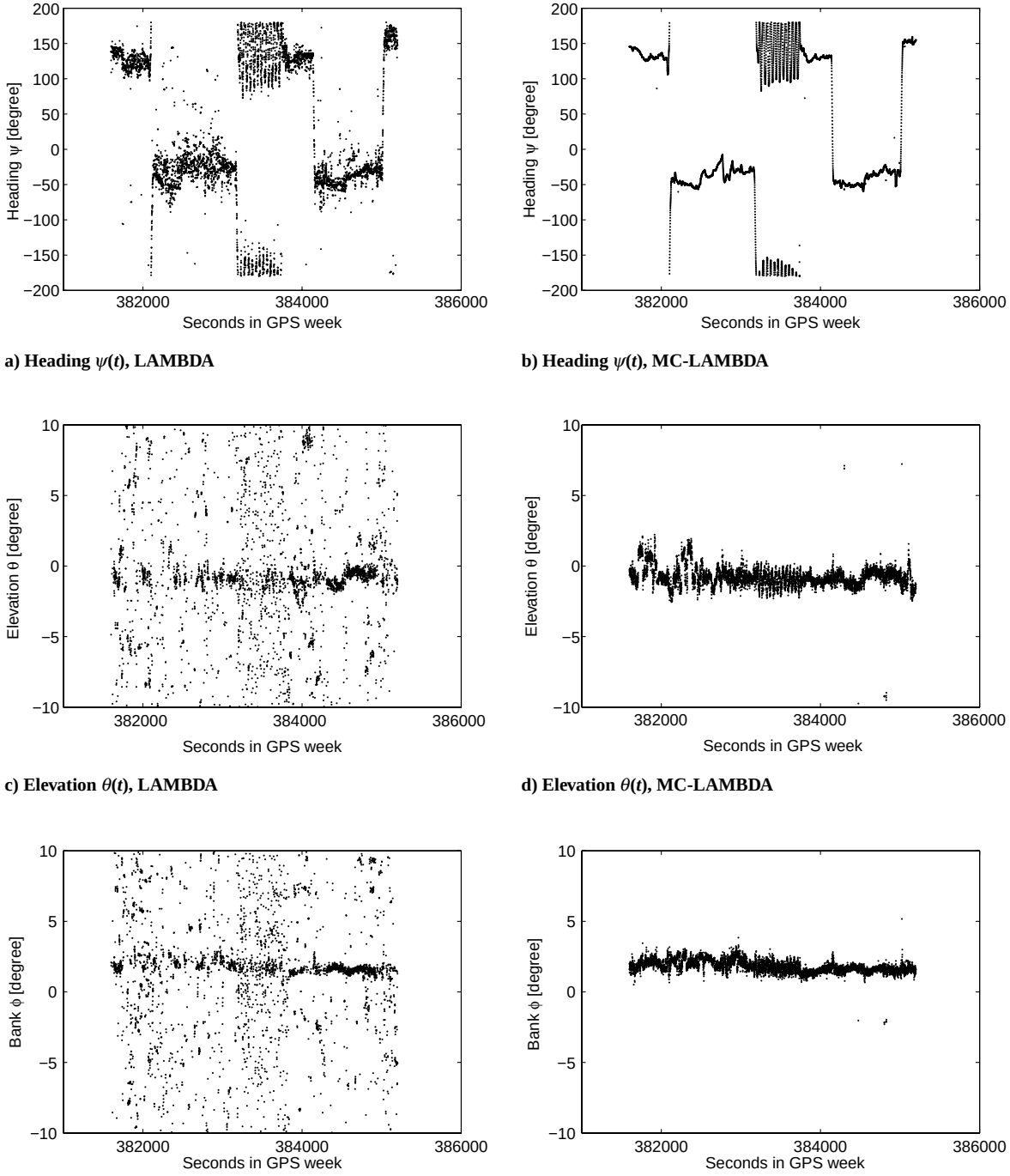

a) Heading $\psi(t)$, LAMBDA

b) Heading $\psi(t)$, MC-LAMBDA

c) Elevation $\theta(t)$, LAMBDA

d) Elevation $\theta(t)$, MC-LAMBDA

e) Bank $\phi(t)$, LAMBDA

f) Bank $\phi(t)$, MC-LAMBDA

Fig. 7 Second boat test: single-epoch full attitude solution, LAMBDA (left) vs MC-LAMBDA (right) method. Attitude is displayed as obtained epoch by epoch, without attempting any validation. The heading time series (Fig. 7b) clearly shows zigzag maneuvers performed by the boat.

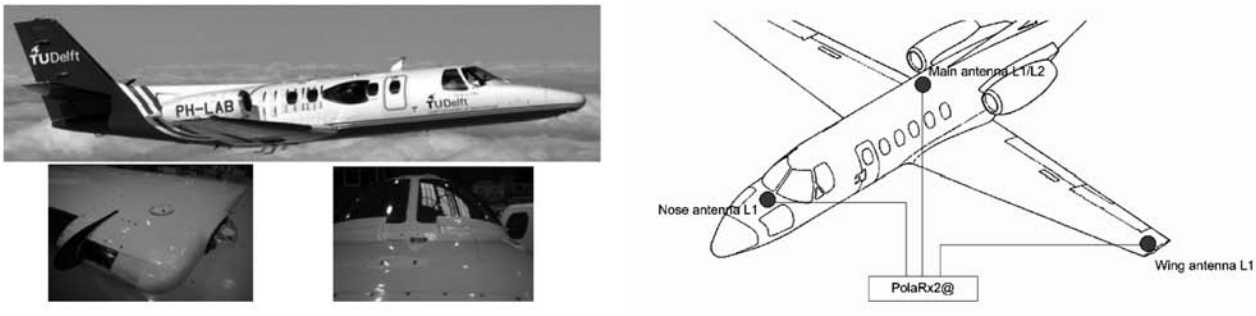

a) Placement of the antennas on the aircraft's body

b) Scheme of the antenna-receiver connections

Fig. 8 Flight test: Cessna Citation II of the Faculty of Aerospace Engineering, Delft University of Technology. Locations of body, wing, and nose antennas are shown.

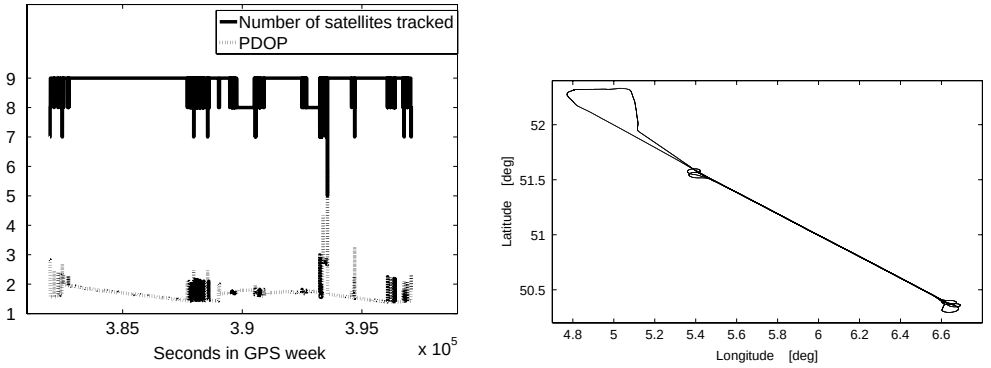

a) Number of satellites tracked and PDOP **b) Groundtrack**

Fig. 9 Cessna Citation II flight test.

Table 10 Flight test: unaided SE–SF success rate (%) for LAMBDA and MC-LAMBDA methods

Baseline	No. SV	LAMBDA	MC-LAMBDA
	Overall	25.1	61.2
Main–nose	8	28.5	78.1
	9	25.0	60.9
	Overall	60.8	93.9
Main–wing	8	31.3	90.4
	9	66.7	94.8
	Two-baseline SE–SF success rate, %		
Main–nose–wing	Overall	24.7	88.1
	8	6.1	92.2
	9	28.6	87.4

Navigation (GAIN) project [70]. The Septentrio PolaRx2 receiver logged data at 10 Hz for the entire duration of the flight, about 4 h. For the processing, the data are downsampled to 1 Hz. The number of available satellites, PDOP values, and the flight trajectory are shown in Fig. 9. The Septentrio receiver was configured to log data from the three antennas (dual frequency on the first one, and single frequency on the two auxiliaries) simultaneously. This limited the number of available channels per antenna to nine, which is therefore the upper limit of the number of commonly tracked satellites. The aircraft also carried an inertial navigation system [INS/initial reference system (IRS) Honeywell LaseRef] onboard. The precise INS output of the three attitude angles is used here to assess the precision of the GNSS-attitude solution.

The unaided SE–SF success rates for the LAMBDA and MC-LAMBDA methods are reported in Table 10. The unconstrained method is capable of fixing the correct set of integer ambiguities for 24.7% of the time, a figure too small to make the standard approach a reliable single-epoch method. Instead, the MC-LAMBDA method confirms the strong performance improvement, being capable of providing the correct integer solution for more than 88% of the epochs. Hence, a precise epoch-by-epoch attitude solution is available for the larger part of the flight duration. Even more interesting, the success rates for the main–nose baseline are lower than for the main–wing baseline. Moreover, with nine visible satellites, the success rate is even lower than with eight satellites for the main–nose baseline, both with the unconstrained and constrained methods. The two-baseline processing shows the same effect. This can be either due to the higher noise levels or due to multipath biases on the observations of one of the satellites tracked, and it is investigated later in this section.

Figure 10 shows the GPS-based attitude angles for the time span considered. The INS solutions are reported as well in order to provide a comparison between the two systems. Table 11 reports the standard

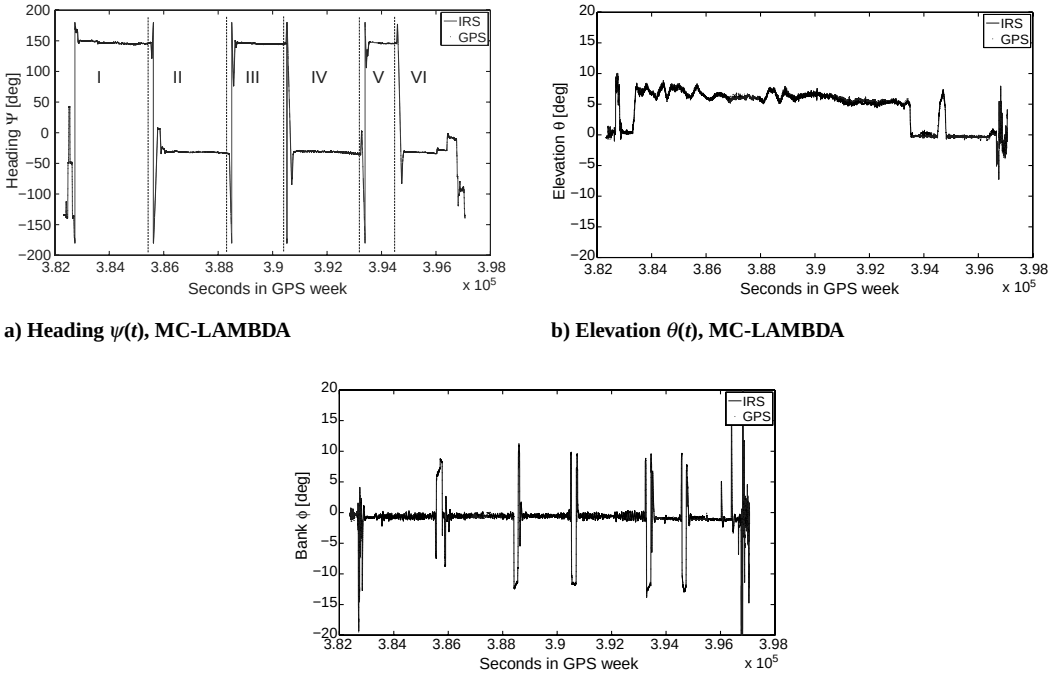

a) Heading $\psi(t)$, MC-LAMBDA **b) Elevation $\theta(t)$, MC-LAMBDA**

c) Bank $\phi(t)$, MC-LAMBDA

Fig. 10 Flight test: time series of the three attitude angles as estimated via GNSS and provided by the INS.

Table 11 Flight test: standard deviations of differences between GPS and INS attitude angle outputs

Parameter	Value, deg
σ_ψ	0.065
σ_θ	0.202
σ_ϕ	0.124

deviations of the differences between the INS and GPS-based attitude solutions. Taking the precise INS output as a benchmark solution, one can conclude that the accuracy obtained is within the expected range, given the baseline lengths involved. The heading angle is estimated with the highest precision, whereas the elevation estimation is characterized by the highest noise levels. This is due to the relative geometry of the antennas and to the fact that the vertical components of the GNSS-based baseline estimations are inherently less accurate than the horizontal components. The bank angle is estimated with higher precision than the elevation angle, being driven by the longer baseline formed by the antennas on the body and on the wing.

As previously mentioned, the single-baseline case main–nose shows a reduced success rate with respect to the baseline main–wing. This can be explained by considering the location of the antenna on the nose: Fig. 8 shows the proximity of the aircraft's cockpit window and two metal panels. This placement caused disturbances, which negatively affected the nose-antenna data. Unfortunately, this effect can not be directly examined, neither with forming the multipath combination [45] (since only single-frequency data are available from the auxiliary antennae) nor with the extracted SNR figure (which does not show any significant effect). Repeating the processing with higher elevation mask angles only marginally improves the success rate, since the redundancy of the observations reduces accordingly. This leads us to consider whether particular directions of the incoming GPS signals are affecting the performance more than others; that is, the combined effect of elevation and azimuth is examined. Figure 10a shows that the aircraft followed a fairly straight trajectory for six time slots, indicated in the figure with roman numbers. During these flight segments, it is found that satellites seen at low elevation and azimuth opposite to the flight direction were introducing biases in the observations. As an example, Fig. 11 reports the carrier phase residuals for the main–nose baseline before and after eliminating satellite pseudorandom noise (PRN) 9 during flight segment III. The reduction of the phase error clearly indicates an improvement in the solution quality, which is also reflected in the capacity of fixing the correct ambiguities: the success rate for this segment increases from 57 to 98% when using the MC-LAMBDA method. Table 12 reports the SE–SF success rates when

Table 12 Flight test: unaided SE–SF success rate (%) for LAMBDA and MC-LAMBDA methods after elimination of those satellites at low elevation and azimuth opposite to the flight direction

Baseline	LAMBDA	MC-LAMBDA
	Single-baseline SE–SF success rate, %	
Main–nose	38.2	91.8
Main–wing	60.8	93.9
	Two-baseline SE–SF success rate, %	
Main–nose–wing	40.3	95.8

the elimination of low-elevation/opposite-azimuth satellites is performed for the whole flight duration. The improvement is evident and demonstrates that a proper placement of the antennas on the aircraft is crucial. On the one hand, it should be such that high-precision attitude solutions can be obtained; but at the same time, the placement should be such that multipath and similar biases are avoided as much as possible.

Another aspect worth mentioning is the problem of platform flexibility. This issue is twofold: the potential problem of incorrect ambiguity estimation and the problem of perturbed attitude determination. If the local body coordinates change due to deformation, then the ambiguity estimation may potentially output incorrect integer ambiguities. However, by means of statistical testing (i.e., testing whether the data fit the imposed geometric constraints), one can test for violation of the geometric constraints. Also, since the principle of integer estimation is a many-to-one mapping, some biases can be allowed in the data without affecting the outcome of integer estimation [71].

The second aspect concerns the attitude determination itself. If the ambiguity resolution outputs wrong ambiguities, then the attitude estimation is biased as well. But even with correct ambiguities, one would obtain biased attitude estimations in case of a deforming platform. Platform flexibility is then an issue for any method that tries to derive the platform attitude from platform-fixed baselines. Only when the baseline local relative geometry is known can the baseline orientations be linked to the platform attitude. In the tests performed, platform flexibility did not affect the method performance.

VI. Conclusions

This work focused on a new rigorous method for GNSS-based attitude determination. The core of the procedure is based on a nontrivial modification of the popular LAMBDA method: the MC-LAMBDA. The MC-LAMBDA method solves for the ambiguities giving proper weighting to the full set of nonlinear geometrical constraints that follow from the a priori knowledge of the relative antenna geometry. These constraints strongly aid the ambiguity

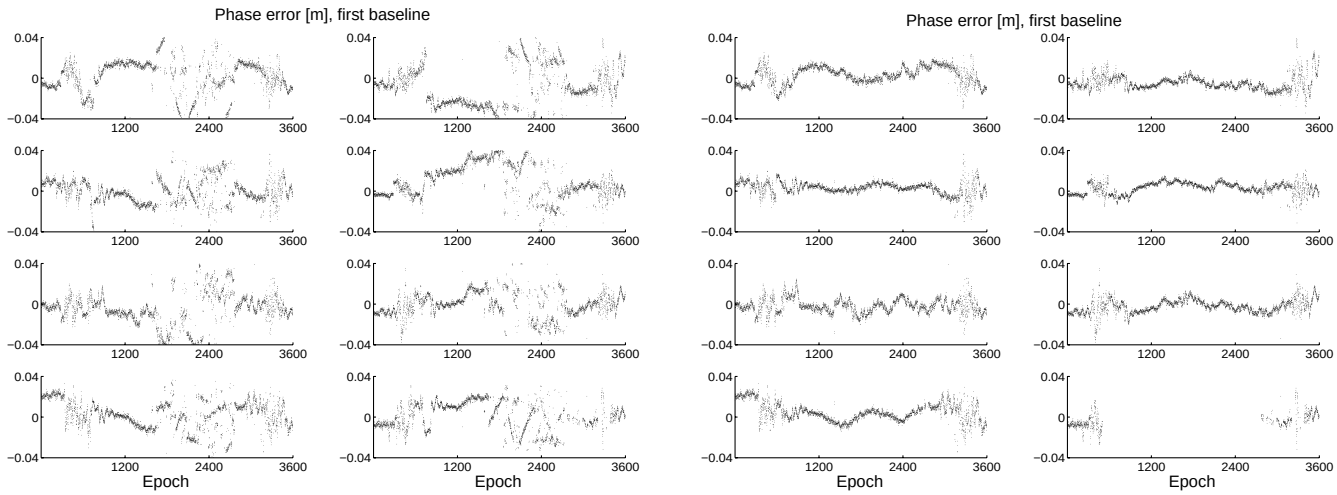

a) DD phase residuals without eliminating satellites **b) DD phase residuals after eliminating satellite PRN 9**

Fig. 11 Test flight 2007: DD phase residuals, first baseline, flight segment III.

resolution process, and they result in an improved capacity of fixing the correct set of carrier phase integer ambiguities.

The proposed method was validated with both simulated data and actual data collected on static, low-dynamic and high-dynamic platforms. In all the data sets examined, the MC-LAMBDA method showed very good performance, thereby largely increasing the SE–SF success rates of the standard LAMBDA method. The improvements are particularly pronounced for the weaker measurement scenarios, e.g., with reduced number of tracked satellites, higher observations noise, and/or biases caused by multipath.

The method of SE–SF GNSS-only performance is emphasized, not only because of the challenges that such models pose but also because of its practical relevance. High-performance single-epoch processing makes the method immune to cycle slips or carrier losses of lock, a quality that is important if platform attitude must be known continuously. Also, single-frequency receivers are used both for low-cost applications and for space-based platforms, where the receivers are limited to a small number of channels due to power limitations, weight constraints, and circuit complexity.

The MC-LAMBDA method also has the advantage of being generally applicable. It is independent of baseline lengths and geometry, independent of platform dynamics, and independent of which GNSSs or combinations thereof are chosen. Moreover, it applies to single- and multi-epoch processing.

An important aspect that still needs to be developed is the theoretical foundation for the probabilistic evaluation of attitude ambiguity resolution. To achieve this, future work will aim at developing the distribution functions for the mixed integer parameters of the attitude model, similar to the existing theory for the unconstrained GNSS model.

Appendix A: Properties of the Vec and Kronecker Product Operators

In the following, vec represents the Vec product operator and $\otimes$ represents the Kronecker product operator:

1) $\mathrm{vec}(ABC) = (C^T \otimes A)\mathrm{vec}(B)$.
2) $(A \otimes B)(C \otimes D) = AB \otimes CD$.
3) $(A \otimes B)^T = A^T \otimes B^T$.
4) $(A \otimes B)^{-1} = A^{-1} \otimes B^{-1}$ (A and B invertible matrices).

Appendix B: Design Matrices Multiplications

$$A^T Q_{yy}^{-1} A = \frac{\lambda^2}{\sigma_\phi^2} Q^{-1}$$

$$A^T Q_{yy}^{-1} G = \frac{\lambda}{\sigma_\phi^2} Q^{-1} B = (G^T Q_{yy}^{-1} A)^T$$

$$G^T Q_{yy}^{-1} G = \frac{\sigma_p^2 + \sigma_\phi^2}{\sigma_p^2 \sigma_\phi^2} B^T Q^{-1} B$$

$$\bar{G}^T Q_{yy}^{-1} \bar{G} = G^T Q_{yy}^{-1} G - G^T Q_{yy}^{-1} A (A^T Q_{yy}^{-1} A)^{-1} A^T Q_{yy}^{-1} G = \frac{1}{\sigma_p^2} B^T Q^{-1} B$$

Appendix C: Simulation Setup

The parameters of the simulation are reported in Table C1.

Table C1 Simulation setup

Parameter	Value
Date, time (GPS week), and location	22 Jan 2008, 00:00 (439), lat: 50°, long: 3°
Frequency (wavelength λ)	L1 (0.19029 m)
Number of satellite (PRNs): PDOP	5 (8,10,15,26,28): 4.192
	6 (8,10,15,26,28,18): 2.142
	7 (8,10,15,26,28,18,9): 1.917
	8 (8,10,15,26,28,18,9,21): 1.811
Undifferenced code noise: σ_p, cm	30–15–5
Undifferenced phase noise: σ_ϕ, mm	30–3–1

Acknowledgments

P. J. G. Teunissen is the recipient of an Australian Research Council Federation Fellowship (project number FF0883188): this support is greatly acknowledged. The research of S. Verhagen is supported by the Dutch Technology Foundation (STW), the applied science division of the The Netherlands Organisation for Scientific Research, and the Technology Program of the Ministry of Economic Affairs. This work has been carried out in the context of the Australian Space Research Program Garada project on synthetic aperture radar formation flying. The authors would like to thank L. Huisman, at the Curtin University of Technology, and C. C. J. M. Tiberius, from the Delft University of Technology (TU Delft), for their support during the experiments described in the paper. The Gravimetry Using Airborne Inertial Navigation experiment team, a mutual cooperation between chairs of Control and Simulation, Physical and Space Geodesy and Mathematical Geodesy and Positioning at TU Delft, is acknowledged for the pleasant cooperation during the flight test.

References

[1] Axelrad, P., and Ward, L., "On-Orbit GPS Based Attitude and Antenna Baseline Estimation," *Proceedings of ION-NTM*, San Diego, CA, Inst. of Navigation, Manassas, VA, 1994, pp. 441–450.

[2] Bar-Itzhack, I. Y., Montgomery, P., and Garrick, J., "Algorithm for Attitude Determination using Global Positioning System," *Journal of Guidance, Control, and Dynamics*, Vol. 21, No. 6, 1998, pp. 846–852. doi:10.2514/2.4347

[3] Brown, R. A., "Instantaneous GPS Attitude Determination," *Proceedings of IEEE Position Location and Navigation Symposium, PLANS 92*, IEEE Publ., Piscataway, NJ, 1992, pp. 113–120.

[4] Cohen, C. E., "Attitude Determination Using GPS," Ph.D. Thesis, Stanford Univ., Palo Alto, CA, 1992.

[5] Crassidis, J. L., Markley, F. L., and Lightsey, E. G., "A New Algorithm for Attitude Determination Using Global Positioning System Signals," *Journal of Guidance, Control, and Dynamics*, Vol. 20, No. 5, 1997, pp. 891–896. doi:10.2514/2.4162

[6] Dai, L., Ling, K. V., and Nagarajan, N., "Real-Time Attitude Determination for Microsatellite by LAMBDA Method Combined with Kalman Filtering," *Proceedings of 22nd AIAA International Communications Satellite Systems Conference and Exhibit 2004 (ICSSC)*, Monterey, CA, AIAA Paper 2004-3118, 2004.

[7] Euler, H. J., "Attitude Determination: Exploiting All Information for Optimal Ambiguity Resolution," *Proceedings of ION GPS*, Inst. of Navigation, Manassas, VA, 1995, pp. 1751–1757.

[8] Hauschild, A., and Montenbruck, O., "GPS-Based Attitude Determination for Microsatellite," *Proceedings of ION GNSS*, Ft, Worth, TX, Inst. of Navigation, Manassas, VA, 2007, pp. 2424–2434.

[9] Kim, D., and Langley, R. B., "GPS Ambiguity Resolution and Validation: Methodologies, Trends and Issues," *7th GNSS Workshop: International Symposium on GPS/GNSS*, Seoul, ROK, Vol. 30, 2000, pp. 1–9, http://gge.unb.ca/gauss/htdocs/papers.pdf/gnss2000.kim.pdf [retrieved 8 July 2011].

[10] Kuylen, L. V., Boon, F., and Simsky, A., "Attitude Determination Methods Used in the PolarRx2 Multi-Antenna GPS Receiver," *Proceedings of ION GPS*, Long Beach, CA, Inst. of Navigation, Manassas, VA, 2005, pp. 125–135.

[11] Li, Y., Zhang, K., Roberts, C., and Murata, M., "On-the-Fly GPS-Based Attitude Determination Using Single- and Double-Differenced Carrier Phase Measurements," *GPS Solutions*, Vol. 8, No. 2, 2004, pp. 93–102. doi:10.1007/s10291-004-0089-3

[12] Madsen, J., and Lightsey, E. G., "Robust Spacecraft Attitude Determination Using Global Positioning System Receivers," *Journal of Spacecraft and Rockets*, Vol. 41, No. 4, 2004, pp. 635–643. doi:10.2514/1.1324

[13] Monikes, R., Wendel, J., and Trommer, G. F., "A Modified LAMBDA Method for Ambiguity Resolution in the Presence of Position Domain Constraints," *Proceedings of ION GPS*, Long Beach, CA, Inst. of Navigation, Manassas, VA, 2005, pp. 18–24.

[14] Psiaki, M. L., "Batch Algorithm for Global-Positioning-System Attitude Determination and Integer Ambiguity Resolution," *Journal of Guidance, Control, and Dynamics*, Vol. 29, No. 5, 2006, pp. 1070–1079. doi:10.2514/1.18351

[15] Schleppe, J., "A Real-Time Attitude System Using a Quaternion Parameterization," *Proceedings of KIS97*, Univ. of Calgary, Banff, AB, Canada, 1997, pp. 395–408.
[16] Bell, T., "Global Positioning System-Based Attitude Determination and the Orthogonal Procrustes Problem," *Journal of Guidance, Control, and Dynamics*, Vol. 26, No. 5, 2003, pp. 820–822. doi:10.2514/2.5117
[17] Cohen, C. E., Lightsey, E. G., and Parkinson, B. W., "Space Flight Tests of Attitude Determination Using GPS," *International Journal of Satellite Communications*, Vol. 12, 1994, pp. 427–433. doi:10.1002/sat.4600120504
[18] Unwin, M., Purivigraipong, S., da Silva Curiel, A., and Sweeting, M., "Stand-Alone Spacecraft Attitude Determination Using Real Flight GPS Data From UOSAT-12," *Acta Astronautica*, Vol. 51, Nos. 1–9, 2002, pp. 261–268. doi:10.1016/S0094-5765(02)00038-3
[19] De Lorenzo, D. S., Alban, S., Gautier, J., Enge, P., and Akos, D., "GPS Attitude Determination for a JPALS Testbed: Integer Initialization and Testing," *Proceedings of IEEE Position Location and Navigation Symposium, PLANS '04*, IEEE Publ., Piscataway, NJ, 2004, pp. 762–770.
[20] Morales-Reyes, A., Haridas, N., Erdogan, A. T., and Arslan, T., "Fault Tolerant and Adaptive GPS Attitude Determination System," *Proceedings of the IEEE Aerospace Conference*, Big Sky, MT, IEEE Publ., Piscataway, NJ, 2009.
[21] Corbett, S., "GPS for Attitude Determination and Positioning in Airborne Remote Sensing," *Proceedings of ION GPS*, Salt Lake City, UT, Inst. of Navigation, Manassas, VA, 1993, pp. 789–796.
[22] Giorgi, G., Teunissen, P. J. G., and Gourlay, T., "Instantaneous GNSS-Based Attitude Determination for Maritime Applications," *IEEE Journal of Oceanic Engineering* (submitted for publication).
[23] Crassidis, J. L., Markley, F. L., and Lightsey, E. G., "Global Positioning System Integer Ambiguity Resolution without Attitude Knowledge," *Journal of Guidance, Control, and Dynamics*, Vol. 22, No. 2, 1999, pp. 212–218. doi:10.2514/2.4395
[24] Misra, P., and Enge, P., *Global Positioning System: Signals, Measurements, and Performance*, 2nd ed., Ganga-Jamuna Press, Lincoln, MA, 2001, pp. 241–250.
[25] Lightsey, E. G., and Crassidis, J. L., "Real Time Attitude Independent GPS Integer Ambiguity Resolution," *Journal of the Astronautical Sciences*, Vol. 52, Nos. 1–2, 2004, pp. 251–267.
[26] Buist, P. J., "The Baseline Constrained LAMBDA Method for Single Epoch, Single Frequency Attitude Determination Applications," *Proceedings of ION GPS*, Ft. Worth, TX, Inst. of Navigation, Manassas, VA, 2007, pp. 2962–2973.
[27] Teunissen, P. J. G., "Least Squares Estimation of the Integer GPS Ambiguities," *Invited Lecture, Section IV Theory and Methodology, IAG General Meeting*, Beijing; also *LGR Series No. 6, Delft Geodetic Computing Center*, Delft Univ. of Technology, Delft, The Netherlands, 1993, pp. 1–12.
[28] Teunissen, P. J. G., "The Least-Squares Ambiguity Decorrelation Adjustment: a Method for Fast GPS Integer Ambiguity Estimation," *Journal of Geodesy*, Vol. 70, Nos. 1–2, 1995, pp. 65–82. doi:10.1007/BF00863419
[29] Boon, F., and Ambrosius, B. A. C., "Results of Real-Time Applications of the LAMBDA Method in GPS Based Aircraft Landings," *Proceedings KIS97*, Univ. of Calgary, Banff, AB, Canada, 1997, pp. 339–345.
[30] Cox, D. B., and Brading, J. D., "Integration of LAMBDA Ambiguity Resolution with Kalman Filter for Relative Navigation of Spacecraft," *Navigation*, Vol. 47, No. 3, 2000, pp. 205–210.
[31] Ji, S., Chen, W., Zhao, C., Ding, X., and Chen, Y., "Single Epoch Ambiguity Resolution for Galileo with the CAR and LAMBDA Methods," *GPS Solutions*, Vol. 11, No. 4, 2007, pp. 259–268. doi:10.1007/s10291-007-0057-9
[32] Huang, S. Q., Wang, J. X., Wang, X. Y., and Chen, J. P., "The Application of the LAMBDA Method in the Estimation of the GPS Slant Wet Vapour," *Acta Aeronautica et Astronautica Sinica*, Vol. 50, No. 1, 2009, pp. 60–68.
[33] Kroes, R., Montenbruck, O., Bertiger, W., and Visser, P., "Precise GRACE Baseline Determination Using GPS," *GPS Solutions*, Vol. 9, No. 1, 2005, pp. 21–31. doi:10.1007/s10291-004-0123-5
[34] Teunissen, P. J. G., "An Optimality Property of the Integer Least-Squares Estimator," *Journal of Geodesy*, Vol. 73, No. 11, 1999, pp. 587–593. doi:10.1007/s001900050269
[35] Teunissen, P. J. G., de Jonge, P. J., and Tiberius, C. C. J. M., "Performance of the LAMBDA Method for Fast GPS Ambiguity Resolution," *Navigation*, Vol. 44, No. 3, 1997, pp. 373–400.
[36] Verhagen, S., and Teunissen, P. J. G., "New Global Navigation Satellite System Ambiguity Resolution Method Compared to Existing Approaches," *Journal of Guidance, Control, and Dynamics*, Vol. 29, No. 4, 2006, pp. 981–991. doi:10.2514/1.15905
[37] Hauschild, A., Grillmayer, G., Montenbruck, O., Markgraf, M., and Vorsmann, P., "GPS Based Attitude Determination for the Flying Laptop Satellite," *Small Satellites for Earth Observation*, Springer, Heidelberg, The Netherlands, 2008, pp. 211–220.
[38] Kuylen, L. V., Nemry, P., Boon, F., Simsky, A., and Lorga, J. F. M., "Comparison of Attitude Performance for Multi-Antenna Receivers," *European Journal of Navigation*, Vol. 4, No. 2, 2006, pp. 1–9.
[39] Wang, C., Walker, R. A., and Feng, Y., "LAMBDA Method for Rigid Body Attitude Determination Based on GPS," *Acta Aeronautica et Astronautica Sinica*, Vol. 22, No. 1, 2001, pp. 61–63.
[40] Teunissen, P. J. G., "Integer Least Squares Theory for the GNSS Compass," *Journal of Geodesy*, Vol. 84, No. 7, 2010, pp. 433–447. doi:10.1007/s00190-010-0380-8
[41] Teunissen, P. J. G., Giorgi, G., and Buist, P. J., "Testing of a New Single-Frequency GNSS Carrier-Phase Compass Method: Land, Ship and Aircraft Experiments," *GPS Solutions*, Vol. 15, No. 1, 2010, pp. 15–28. doi:10.1007/s10291-010-0164-x
[42] Teunissen, P. J. G., "Multivariate Mixed Integer Least-Squares Estimation: Theory and Applications," *Journal of Geodesy* (submitted for publication).
[43] Wang, B., Miao, L., Wang, S., and Shen, J., "A Constrained LAMBDA Method for GPS Attitude Determination," *GPS Solutions*, Vol. 13, No. 2, 2009, pp. 97–107. doi:10.1007/s10291-008-0103-2
[44] Hodgart, M. S., and Purivigraipong, S., "New Approach to Resolving Instantaneous Integer Ambiguity Resolution for Spacecraft Attitude Determination Using GPS Signals," *Proceedings of IEEE Position Location and Navigation Symposium, PLANS '00*, IEEE Publ., Piscataway, NJ, 2000, pp. 132–139.
[45] Teunissen, P. J. G., and Kleusberg, A., "*GPS for Geodesy*," 2nd ed., Springer, New York, 1998, Chap. 5.
[46] Teunissen, P. J. G., "A Canonical Theory for Short GPS Baselines. Part I: The Baseline Precision," *Journal of Geodesy*, Vol. 71, No. 6, 1997, pp. 320–336. doi:10.1007/s001900050100
[47] Teunissen, P. J. G., "A Canonical Theory for Short GPS Baselines. Part II: the Ambiguity Precision and Correlation," *Journal of Geodesy*, Vol. 71, No. 7, 1997, pp. 389–401. doi:10.1007/s001900050107
[48] Teunissen, P. J. G., "A Canonical Theory for Short GPS Baselines. Part III: the Geometry of the Ambiguity Search Space," *Journal of Geodesy*, Vol. 71, No. 8, 1997, pp. 486–501. doi:10.1007/s001900050117
[49] Teunissen, P. J. G., "A Canonical Theory for Short GPS Baselines. Part IV: Precision Versus Reliability," *Journal of Geodesy*, Vol. 71, No. 9, 1997, pp. 513–525. doi:10.1007/s001900050119
[50] Battin, R. H., "An Introduction to the Mathematics and Methods of Astrodynamics," *AIAA Education Series*, AIAA, New York, 1987, pp. 80–94.
[51] Shuster, M. D., "A Survey of Attitude Representations," *Journal of the Astronautical Sciences*, Vol. 41, No. 4, 1993, pp. 439–517.
[52] Verhagen, S., and Joosten, P., "Analysis of Integer Ambiguity Resolution Algorithms," *European Journal of Navigation*, Vol. 2, No. 4, 2004, pp. 38–50.
[53] Teunissen, P. J. G., "Influence of Ambiguity Precision on the Success Rate of GNSS Integer Ambiguity Bootstrapping," *Journal of Geodesy*, Vol. 81, No. 5, 2007, pp. 351–358. doi:10.1007/s00190-006-0111-3
[54] Teunissen, P. J. G., "The Success Rate and Precision of GPS Ambiguities," *Journal of Geodesy*, Vol. 74, No. 3, 2000, pp. 321–326. doi:10.1007/s001900050289
[55] Giorgi, G., Teunissen, P. J. G., and Buist, P. J., "A Search and Shrink Approach for the Baseline Constrained LAMBDA: Experimental Results," *Proceedings of the International Symposium on GPS/GNSS 2008*, edited by A. Yasuda, Tokyo Univ. of Marine Science and Technology, Tokyo, 2008, pp. 797–806.
[56] Wertz, J. R., *Spacecraft Attitude Determination and Control*, D. Reidel Publ., Dordrecht, The Netherlands, 1978, Chap. 12.
[57] Wahba, G., "Problem 65-1: A Least Squares Estimate of Spacecraft Attitude," *SIAM Review*, Vol. 7, No. 3, 1965, pp. 384–386.
[58] Schonemann, P. H., "A Generalized Solution of the Orthogonal Procrustes Problem," *Psychometrika*, Vol. 31, No. 1, 1966, pp. 1–10.

doi:10.1007/BF02289451
[59] Davenport, P. B., "A Vector Approach to the Algebra of Rotations with Applications," NASA TN D-4696, Goddard Space Flight Center, 1968.
[60] Shuster, M. D., "Approximate Algorithms for Fast Optimal Attitude Computation," *AIAA Guidance and Control Conference*, Palo Alto, CA, AIAA Paper 1978-1249, 1978.
[61] Shuster, M. D., and Oh, S. D., "Three-Axis Attitude Determination from Vector Observations," *Journal of Guidance, Control, and Dynamics*, Vol. 4, No. 1, 1981, pp. 70–77. doi:10.2514/3.19717
[62] Markley, F. L., and Landis, F., "Attitude Determination Using Vector Observations: a Fast Optimal Matrix Algorithm," *Journal of the Astronautical Sciences*, Vol. 41, No. 2, 1993, pp. 261–280.
[63] Mortari, D., "ESOQ: A Closed-Form Solution to the Wahba Problem," *Journal of the Astronautical Sciences*, Vol. 45, No. 2, 1997, pp. 195–204.
[64] Mortari, D., "Second Estimator of the Optimal Quaternion," *Journal of Guidance, Control, and Dynamics*, Vol. 23, No. 5, 2000, pp. 885–888. doi:10.2514/2.4618
[65] Markley, F. L., and Mortari, D., "How to Estimate Attitude from Vector Observations," *AAS/AIAA Astrodynamics Specialist Conference*, American Astronomical Soc. Paper 99-427, Washington, D.C., 1999.
[66] Markley, F. L., and Mortari, D., "Quaternion Attitude Estimation Using Vector Observations," *Journal of the Astronautical Sciences*, Vol. 48, Nos. 2–3, 2000, pp. 359–380.
[67] Cheng, Y., and Shuster, M. D., "Robustness and Accuracy of the QUEST Algorithm," *Advances in the Astronautical Sciences*, Vol. 127, American Astronautical Soc., Washington, D.C., 2007, pp. 41–61.
[68] Vapnyarskii, I. B., "Lagrange multipliers," *Hazewinkel, Michiel, Encyclopaedia of Mathematics*, Springer, New York, 2001.
[69] Teunissen, P. J. G., "Nonlinear Least Squares," *Manuscripta Geodaetica*, Vol. 15, 1990, pp. 137–150.
[70] Alberts, B. A., Gunter, B. C., Muis, A., Chu, Q. P., Giorgi, G., Huisman, L., Buist, P. J., Tiberius, C. C. J. M., and Lindenburg, H., "Correcting Strapdown GPS/INS Gravimetry Estimates with GPS Attitude Data," *Proceedings of the International Symposium on Gravity, Geoid and Earth Observation, GGEO 2008*, Chania, Crete, Greece, Springer, New York, 2010, pp. 93–100. doi:10.1007/978-3-642-10634-7_13
[71] Teunissen, P. J. G., "Integer Estimation in the Presence of Biases," *Journal of Geodesy*, Vol. 75, Nos. 7–8, 2001, pp. 399–407. doi:10.1007/s001900100191